A DYNAMIC MODEL OF THE ATOMIZATION MECHANISM IN THE INDUCTIVELY COUPLED PLASMA

BY

KIGH-SHONE YEAH

A DISSERTATION PRESENTED TO THE GRADUATE SCHOOL
OF THE UNIVERSITY OF FLORIDA IN
PARTIAL FULFILLMENT OF THE REQUIREMENTS
FOR THE DEGREE OF DOCTOR OF PHILOSOPHY

UNIVERSITY OF FLORIDA

1987

To my parents and my wife,

whose loving support made all this possible.

ACKNOWLEDGMENTS

I wish to express my sincere appreciation to Dr. Shaw-Chii Wu, Mr. Yuan-Ko Chang, and Mr. Rong-Gian Lee for their favorable arrangements of this advanced study. In particular, a special expression of gratitude must be made to Mr. Chi-Chuen Jan for his enthusiastic assistance and spiritual encouragement.

I also wish to thank Dr. Benjamin W. Smith and Dr. Michael J. Rutledge for their instrumentation set-up and computer data processing used in this work.

Many thanks are extended to Dr. Kuang-Pang Li for his theoretical discussion and comments, to Dr. David J.D. Huang for his experimental assistance, and to Mr. Tiing Yu for his computer simulation programmings.

My hearty gratitude is also extended to my research director, Dr. James D. Winefordner, for giving me the privilege of performing this work. During the past five years, his many opportune assistances have become my everlastingly unforgettable memory.

Special thanks must be given to my wife. Without her encouragement and patience, this work would not have been possible.

TABLE OF CONTENTS

Page

ACKNOWLEDGMENTS....................iii

ABSTRACT....................vi

CHAPTERS

1 INTRODUCTION....................1

Historical Development of Inductively Coupled Plasma Spectrometry....................3
Review and Comments of the Proposed Excitation Mechanisms in an Inductively Coupled Plasma....................7

2 A DYNAMIC MODEL USING THE STOCHASTIC APPROACH FOR THE ELUCIDATION OF ANALYTE ATOMIZATION MECHANISM IN AN INDUCTIVELY COUPLED PLASMA....................17

Introduction....................17
Theoretical Considerations....................19
- The Stochastic Approach....................19
- The Dynamic Model....................24
- Solution of Rate Equations....................26
- Evaluation of Rate Constants....................34

Experimental....................35
Results and Discussion....................38

3 ESTIMATION OF RATE CONSTANTS USING STATISTICAL MOMENTS OF SPATIALLY RESOLVED SIGNAL PROFILES FOR THE ELUCIDATION OF ANALYTE ATOMIZATION MECHANISM IN AN INDUCTIVELY COUPLED PLASMA....................68

Introduction....................68
Theoretical Considerations....................70
Experimental....................75
- Instrumental Set-Up....................75
- Method of Calculation....................75
- Operational Conditions....................77

Results and Discussion....................77

4 CONCLUSIONS AND FUTURE WORK............................107

APPENDICES

A EXPANSION DUE TO ANALYTE DIFFUSION AND CHEMICAL REACTIONS...115

B SOLUTION OF RATE CONSTANTS..............................121

C PROGRAM FOR COMPUTER SIMULATION.........................126

D PROGRAM FOR STATISTICAL MOMENTS CALCULATION............127

E PROGRAM TO CALCULATE RATE CONSTANTS IN INDUCTIVELY COUPLED PLASMA...128

F PROGRAM FOR GETTING DATA FROM SR 265 BINARY TO ASCII...130

REFERENCES...131

BIOGRAPHICAL SKETCH..138

Abstract of Dissertation Presented to the Graduate School
of the University of Florida in Partial Fulfillment of the
Requirements for the Degree of Doctor of Philosophy

A DYNAMIC MODEL OF THE ATOMIZATION MECHANISM IN THE INDUCTIVELY COUPLED PLASMA

BY

KIGH-SHONE YEAH

August, 1987

Chairman: James D. Winefordner
Major Department: Chemistry

A general dynamic model treated by a stochastic approach is established. In this model, kinetics of rate-determining reactions such as dissociation, atomization, ionization, and recombination are considered. For mathematical simplification, it is imagined that the vapor plume results from a single aerosol droplet and the kinetic processes taking place are then closely followed. Under constant pressure, diffusion is approximated as volume expansion. The resultant analyte distribution observed should then be a good approximation to the real situation, assuming an inductively coupled plasma with reproducible experimental conditions and a uniform solution droplet size distribution. The spatially resolved atomic and ionic profiles are characterized by their statistical moments. The evaluation of the zeroth and first moments allows estimation of reaction rate constants. By comparison of the simulated profiles using different rate constants with the experimental axial signal profiles, analyte atomization can be more precisely described.

CHAPTER 1
INTRODUCTION

The inductively coupled plasma (ICP) can be simply described as a volume of partially ionized gas (usually argon) inductively coupled to high radio frequency (rf) radiation (5-50 MHz). The plasma is sustained in a torch usually consisting of three concentric quartz tubes through which coolant gas is supplied to prevent melting of the torch by the plasma, plasma gas is supplied to sustain the plasma, and an injector gas flow is supplied to facilitate sample introduction. High-frequency power is applied via an induction coil (fabricated from copper tubing to facilitate water cooling) in which the plasma torch is mounted and enables the plasma to become self-sustaining through a series of atomization, ionization, and excitation mechanisms once the plasma has been initiated.

The figures of merit in analytical utility of the ICP consist of detection limits, degree of freedom from interelement interferences, and signal-to-background and signal-to-noise ratios. Detection limits for many elements in the ICP are in the ppb range, and linear dynamic ranges usually are over 5-6 orders of magnitude with respect to analyte concentration, permitting element determinations to be undertaken at a single dilution of the sample. As the plasma is sustained without the use of supporting electrodes, the background is relatively clear, consisting of only excited Ar lines and weak molecular band emission for species such as OH, CN, NO and N_2.

In addition, the ICP has a high sensitivity for ion lines, a good signal-to-background ratio, and reduced interelement interferences compared with other excitation sources. However, interelement interferences, which are small, still do exist in the ICP. The mechanism involved in excitation of the ICP are not well understood. Many contradicting points of view have arisen in the literature concerning the magnitude and reason for interferences as well as the excitation mechanisms involved. To elucidate the spatial dependence of emission and interference effects, it is important to know the possible atomization, ionization, and excitation mechanisms that might occur in the ICP. The plasma is not homogeneous with respect to temperature because it is formed from a flowing stream of supporting gas that sweeps plasma matter consisting of ions, electrons, and neutral atoms away from the energy input region (within and near the induction coil). The spatial dependencies of the emission intensity of many atom and ion lines can be linked in some instances with the temperature inhomogeneity, but in other instances, it is necessary to study the role of atomization mechanisms which are kinetic in nature. The ICP plasma is not in complete local thermal equilibrium (LTE). The non-LTE phenomena have been a key point in the studies on characterization and excitation mechanisms of the ICP. Much research has been carried out by means of the measurements of physical and spectral parameters of the ICP. From these experimental data as well as some theoretical considerations, several excitation mechanisms of the analyte species have been proposed since Mermet's proposal of the Penning ionization processes with argon metastable atom. It should be noticed that these proposals or hypotheses cannot successfully interpret global processes concerning atomization, ionization, and excitation mechanisms in the plasma.

Historical Development of Inductively Coupled Plasma Spectrometry

During the fall and winter of 1941 to 1942 in Leningrad, Babat [1,2] first succeeded in maintaining induction heated plasmas at atmospheric pressure with power inputs as high as 30-50 kW. He described capacitative coupled electrodeless discharges excited by an electric field and eddy electrodeless discharges excited by an alternating magnetic field in a closed system. His conclusions are as follows. The higher the frequency of the generator, the lower the current and power consumption required to form a stable plasma. The higher the inductive leakage resistance between the inductor and the "gaseous turn," the lower the current and power consumption for stability. He had in mind industrial applications of rf discharges for electrochemistry of gases; heating and fusion of fireproof materials; and creating high-intensity, economic light sources.

Stabilization of an inductively heated plasma discharge operated at atmospheric pressure and in gases flowing through an open-ended tube was achieved in the early 1960s. Reed [3-5] was the first to generate such a discharge, which he designed with the major purpose of crystal growing, although he suggested that the ICP discharge could be useful as a spectroscopic light source.

Two groups were stimulated by Reed's publication to begin work independently toward spectrochemical use of an ICP discharge. Fassel [6,7] and Greenfield [8] recounted their initial analytical studies of ICPs in 1962; the first results of which were reported in 1964 [9] and 1965 [10]. Both of them felt that Reed's "plasma torch" offered, in principle, unique potential as a high-temperature atomization-excitation source, free of contamination from electrode vapors. Mainly through the efforts by the groups of Greenfield [9,11-13] and Fassel [10,14-16] during the 1960s and early 1970s, the ICP has become a commercially available product and a viable spectroanalytical tool. In the same period of time, other researchers have also explored [17-28] the potentialities of ICPs for spectrochemical analysis.

One criterion of the progress in the early years was the improvement in the detection limits. The paper of Dickinson and Fassel [14], published in 1969, proclaimed a new era in ICP-atomic emission spectrometry (ICP-AES). They succeeded in reducing the detection limits to the 0.1-10 ng/ml range for many elements, which meant an improvement by two or more orders of magnitude compared to the results achieved previously. This publication stands as a significant landmark paper in ICP progress [20].

Dickinson and Fassel exploited the skin-depth effect of high-frequency currents and also profiled their ICP arrangement in such a way that a toroidal instead of an ellipsoid ("tear drop") discharge was formed. Therefore, the sample could be effectively introduced through the central channel of the toroid. The aerosol was generated with an ultrasonic nebulizer and desolvated prior to its introduction into the plasma. The high efficiency of ultrasonic nebulizer contributed to the success of the efforts.

By 1971, the major advantages of ICPs as excitation sources for AES had been reported and were summarized by Fassel [15] as follows: (a) effective injection of the sample into the hot portion of the plasma; (b) relatively long-residence time of the sample in the plasma; (c) higher temperature than combustion flames; (d) continuous temperature gradient from 9000°K to room temperature, allowing greater latitude in selecting optimal temperature; (e) free atoms may be generated in the hottest zones of the plasma and then observed in lower temperature zones where background emission is lower; (f) chemical environment may be manipulated, within limits; and (g) no electrode contamination.

The consequences reported by Dickinson and Fassel were proved independently in 1972 by Souilliart and Robin [29] and Boumans and de Boer [30] using different ICP instruments and operating conditions. The potentials of low-power argon ICPs as excitation sources for simultaneous multielement analysis employing "compromise operating conditions" were recognize and firmly established [30-33]. Other noted, exploited, and documented figures of merit [29,32,34] include extremely high sensitivity of ionic lines in the emission spectra, low-interference levels under judiciously chosen operating conditions, large dynamic range, and fair stability. These results, along with those of the early efforts, form the basis of present-day ICP-AES.

Greenfield and his co-workers followed a different line to study the ICPs. They employed the high-power nitrogen-argon ("nitrogen cooled") ICPs, of which higher sensitivity, smaller liability to interferences, and better precision were postulated to be major advantages in comparison to low-power argon ICPs [35,36]. The past has seen many--often confusing--arguments in favor of either low-power argon or high-power nitrogen-argon ICPs, but it is only since rather recently that clear experimental data are beginning to clarify the complex picture.

Montaser et al. [37,38] performed optimization studies on a plasma with pure N_2 as outer gas and argon as intermediate and carrier gas, and varied the power and the gas flow rates. They agreed with Ebdon et al. [39] that, for N_2-Ar ICPs, it is more difficult to find good compromise conditions than for a low-power argon ICP and found the "sensitivity advantage" (higher net line intensities) in N_2-Ar ICPs did not translate into improved detection limits because of the higher background.

The confusion about the arguments of the two categories of ICPs did not detract from the research of Greenfield's group. They stated in 1975 that they had been using the high-power nitrogen-argon ICP system on a daily routine basis for practical analysis of a large variety of samples during the past four years. The usefulness of this type of ICPs has also been documented by Greenfield and his group [8,9,35,36] and by Watson [40-43], Ohls [44-46], Broekaert

[47-51] and their associates. Although various applications of low-power argon ICPs had been reported by 1975 [31,52-55], the era of widespread use of these ICPs for practical applications was just beginning with the advent of commercial instruments.

The first modern commercial ICP emission spectrometric instrument was introduced in 1974 by the Applied Research Laboratories (Sunland, CA) [56,57] and this was followed in 1975 by an instrument produced by the Jarrell Ash Division of Fisher Corporation (Waltham, MA). As commercial instrumentation has become available, rather explosive developments were to follow. Emphasis in ICP research shifted from demonstrating powers of detection to elucidating other performance characteristics such as reliability, stability, precision, and accuracy needed for daily routine analysis.

Assessing the position of ICP-AES, Winefordner et al. [58], Boumans and de Boer [30,59], Sharp [60], Fassel et al. [31,61], and Greenfield et al. [35] agreed that the ICP might well become one of the best characterized and most effectively applied spectrochemical sources yet discovered. According to Barnes' evaluation [62], ICP-AES will probably not reach in the 1980s the stage in which it will be gradually replaced by other methods with greater speed, economy, convenience, sensitivity, and selectivity.

Review and Comments of the Proposed Excitation Mechanisms in an Inductively Coupled Plasma

The major goal of the diagnostic research on the ICP is to elucidate the excitation mechanisms for sustaining argon gas and analyte introduced into the plasma. As mentioned before, one of the features of the ICP is that it is not in LTE. Local thermal equilibrium exists in a system when all temperature-dependent processes (e.g., the Boltzmann population distribution and the Maxwell velocity distribution function) can be described by a single temperature for the system. It also implies that all radiative processes are balanced by absorptive properties in the local environment of the plasma and hence little or no emission would be observed. The non-LTE phenomena became apparent soon after the introduction of the ICP as an emission source when researchers began to characterize the discharge. Different temperatures were found depending on the spectroscopic technique used to determine the temperature. Moreover, the ratio of the intensity of ion lines to atom lines of the same element were found to be much greater when compared with theoretical ratios determined assuming LTE. These results coupled with the fact that the more energetic emission lines had their maximum emission intensities higher in the plasma relative to the less energetic lines that led spectroscopists to seek an explanation for these observations. Mermet [34,63] was the first to suggest that ionization temperature, T_{ion}, excitation temperature, T_{exc}, electron temperature, T_e, and rotational temperature, T_{rot}, were significantly different and that LTE did not exist in the ICP. Many other investigators have confirmed his suggestion [34,63-73]; we can realize the statement that "the argon ICP under normal operating conditions is not in LTE" as a fact, although it may be approached under certain conditions.

Walter et al. [68] measured T_{ion}, T_{exc} and T_e in a 144 MHz ICP and found in their plasma that T_{ion} was lower than T_{exc}, while T_e was an order of magnitude larger than T_{exc}. The latter difference in temperatures was attributed to a longer mean free path of electrons resulting in higher kinetic energy. Therefore, the population of higher energy levels arose from energy transfer from the kinetically energetic electrons resulting in higher temperature.

Mermet [34] first postulated Penning ionization as an explanation for the high detection power attained with ion lines. Penning ionization consists of ionization and excitation of analyte atoms through interaction with excited metastable argon atoms (these atoms have high excitation energy, 11.55 and 11.76 eV). The process may be represented by

$$Ar^m + X \rightarrow Ar + X^+ + e^- \qquad (1-1)$$

and

$$Ar^m + X \rightarrow Ar + X^{+*} + e^- \qquad (1-2)$$

The reverse processes of Eqs. (1-1) and (1-2) were negligible on the assumption that Ar^m was overpopulated. This mechanism apparently provides higher population ions; however, it cannot be applied to ionic levels for which the ionization plus excitation energy is higher than the excitation energy of Ar^m. In this case, a two-step reaction including electron collision should be considered:

$$Ar^m + X \rightarrow Ar + X^+ + e^- \qquad (1\text{-}3)$$

$$X^+ + e^- \rightarrow X^{+*} + e^- \qquad (1\text{-}4)$$

The overpopulation of higher atomic levels can be described in terms of the direct excitation by Ar^m or the recombination of the overpopulated ionic ground state with electrons (three-body recombination).

$$Ar^m + X \rightarrow Ar + X^* \qquad (1\text{-}5)$$

$$X^+ + 2e^- \rightarrow X^* + e^- \qquad (1\text{-}6)$$

Boumans and de Boer [66] also postulated that Ar^m acts as an ionizer (Penning ionization) as well as an ionizant (easily ionizable element, EIE) which acts as follows:

$$Ar^m + e^- \rightarrow Ar^+ + 2e^- \qquad (1\text{-}7)$$

Therefore, the electron number density in the plasma increases. (Levels of Ar^m, $^3P_0$ and $^3P_2$ have a relatively low ionization potential of about 4 eV.) They also pointed out that deviation from LTE was favorable resulting in high sensitivity of ionic lines and a relatively low ionization interference interrelated with the overpopulation of Ar^m. Such an overpopulation is a result of the mixing of cold carrier gas and hot plasma gas which is responsible for the suprathermal population of ionic levels (Penning ionization) and the high suprathermal electron number density. (Overpopulation of Ar^m occurs because of their extended lifetimes compared with the lifetimes of the excited states [74]; the Ar^m do not spontaneously return to the ground state through a radiative transition but remain in the metastable state where excitation energy is then transferred by the Penning ionization process.)

Edmonds and Horlick [75] pointed out that the Penning ionization mechanism would result in (a) ion line emission not occurring until Ar^m diffused into the central analyte channel, relatively high in the plasma discharge; (b) spatial emission patterns of ionic species generated by Penning ionization would be species independent; and (c) a significant decrease in ion line emission as nebulizer flow-rate is increased. From the above observation, they concluded that, in the lower region, analyte was excited by electron impact process while in the upper region by Penning ionization. The required practical support for the existence of metastable levels in the upper region of the plasma was given by Nojiri et al. [73] and Uchida et al. [76] who found Ar^m clearly exists even at a distance of 8 mm from the plasma center and at a height of 7.5 mm, and the density of Ar^m at the outer positions was higher than at the center of the plasma at a height of 3.5 mm. However, the Penning ionization process cannot explain the sensitive lines of several elements which have a total excitation energy higher than the excitation energy of the metastable argon atoms. Moreover, recent measurements [77] confirmed that the number density of metastable argon was, about 10^{12} cm^{-3}, i.e., no overpopulation. This result appears to be the most serious contradiction against the Penning ionization mechanism [78,79].

In recent years, a charge transfer reaction has been proposed [80,81] since the number density of argon ion is of the order of 10^{15} cm^{-3} with the assumption of electrical neutrality of the plasma, which is three orders of magnitude higher than that of metastable argon. Therefore,

$$Ar^{+} + X \rightarrow Ar + X^{+} \qquad (1\text{-}8)$$

$$Ar^{+} + X \rightarrow Ar + X^{+*} \qquad (1\text{-}9)$$

where ionization (plus excitation) potential of X must be lower than that of Ar (15.76 eV). These processes help us to explain the non-LTE phenomena of the ICP similar to the Penning ionization phenomena. In addition, a larger population of argon ion favors this mechanism. The major drawback of this process is that the reverse reaction of Eq. (1-8) was neglected, i.e.,

$$Ar + X^{+} \rightarrow Ar^{+} + X \qquad (1\text{-}10)$$

There is a possibility that the number density of analyte ions is reduced through collisions with highly populated ground state argon atoms, which are estimated to be in the order of 10^{18} cm^{-3}.

Similar to the case of Penning ionization, this process is not able to populate levels with a total excitation energy higher than the ionization energy of argon (15.76 eV). This is also a departure from the observed facts.

Boumans [82] considered a recombining plasma model put forward by Fujimoto [83-86] and suggested the excited argon atoms, Ar^*, not just Ar^m, are involved in Penning ionization reactions and ion-electron recombination plays a vital role in creating excited level populations. His mechanism can be described by Penning ionization with excited argon atom, three-body recombination, and spontaneous emission in both of the atomic and ionic levels. In his model, the importance of Penning ionization far exceeded the electron impact ionization. This point of view seems to be doubtful and needs to be further assessed.

The recombining plasma model allows easy interpretation of the overpopulation of ions, but cannot offer any suggestion for the overpopulation of higher excited states.

Aeschbach [87] suggested that the two main causes of non-LTE behavior are due to (a) the kinetic energy of the electrons--resulting from the radiofrequency power input of the field--being higher than the kinetic energy of the gas particles and (b) ambipolar diffusion of electrons as a consequence of extremely high gradients in electron density and temperature distribution. He postulated that electrons which were created in the hot plasma ring inside and above the plasma ring proceeded axial convection and ambipolar diffusion. Ambipolar diffusion arises because electrons move faster than ions, resulting in a charge separation which produces an electric field that exerts its force to increase the drift velocity of the ions and retard the drift velocity of the electron. However, as he admitted, this diffusion model cannot explain the relative population of various energy levels of one species and the increase of excitation temperature with excitation energy.

Recently, the radiation trapping model was proposed by Blades and Hieftje [88]. They suggested that the argon atoms in metastable states and in adjacent radiative states equilibrated rapidly through collisions with ground state argon atoms. The ground state atoms in the cool central zone absorbed the resonance radiation emitted from the surrounding hot zone. At atmospheric pressure, this exchange of energy (emission from one atom which is then reabsorbed by another atom) can occur many times before such radiation escapes from the boundaries of the enclosed gas. This trapped radiation, which leads to longer lifetimes (~ 1 ms) for the radiating levels, effectively acts as a storage of excitational energy in the enclosing gas.

Coupling the radiation trapping model with the hypothesis of Boumans and de Boer [66], Blades [89] postulated a mechanism of "assisted ionization." According to his proposal, the populations of the radiative and metastable atoms in the aerosol channel are enhanced by radiation trapping in the hot annular zone, and the overpopulated excited levels "assist" the ionization of neutral argon. This results in the suprathermal population of electrons in the central core. The overpopulation of analyte ions is interpreted by the response of the ionization equilibrium to the excess population of electrons.

In a later paper, Mills and Hieftje [90] reconsidered radiation trapping and revised the apparent lifetime for the metastable states of only 1.6 μs. They conceded that radiation trapping, which was only significantly responsible for sustaining the plasma within the load coil region and could not be considered as a mechanism for the apparent concentration of Ar^m above the load coil of the ICP.

Recently, a quantitative model of excitation which considers various reactions as the rate processes occurring in the plasma have been attempted. These workers [91-95] considered the rates for all processes that involved excitation, de-excitation, ionization, recombination, ambipolar diffusion, and convection of the plasma species and electrons. The number density of argon energy states can be calculated under the steady-state approximation.

According to a recent calculation for the excitation of Mg and Cd by a collisional-radiative model [96], in which the Penning ionization and charge transfer processes were taken into account, neutral atoms in all energy levels and ions in lower levels are overpopulated. A further comparison of reaction rates leads to the conclusion that the main mechanism for analyte ionization is the electron impact process.

The collisional-radiative model, which includes the other mechanisms suggested previously, seems to be the most suitable to elucidate the excitation mechanisms in the ICP; however, it has not been proved yet. The effectiveness of this model still depends on the coincidence between the experimental data for the plasma properties and the theoretical calculations, such as absolute number densities and effective lifetimes of various energy levels.

Almost all of the above models were built on the basis of LTE [32,34,63,66,69,71,73,76,80,82,89,97-99] or near LTE (i.e., partial-LTE or p-LTE) [32,66,80,98,99]. As mentioned at the beginning of this section, LTE has been diagnosed not to exist throughout the ICP [32,63,66,69,71,89,97,99,100,101]. The non-LTE phenomena render the proposed models less than adequate for mechanistic elucidation of analyte atomization and excitation.

A more general dynamic model is proposed by the author, where all processes are considered kinetic ones which lead to time- (or height-) dependent distributions of analyte species. The treatment of the kinetic model employs a stochastic approach. Spatial axial distributions of theoretically simulated and experimental distributions of analyte atoms and ions are compared. Measurements of experimental height profiles and evaluation of statistical moments allows estimation of reaction rate constants.

CHAPTER 2
A DYNAMIC MODEL USING THE STOCHASTIC APPROACH FOR THE EVALUATION OF ANALYTE ATOMIZATION MECHANISM IN AN INDUCTIVELY COUPLED PLASMA

Introduction

Within the past 12 years, many workers have devoted themselves to the elucidation of analyte atom and ion excitation mechanisms in the inductively coupled plasma (ICP) [34-101]. A great many observations have been performed by the space-resolved spectrometry, and many speculative models have been proposed. Those featuring Penning ionization [34,66,75], charge transfer reaction [80,81], recombining plasma [82-86], ambipolar diffusion [87], radiation trapping [88-90] and collisional-radiative [91-96] are the most popular ones. Almost all the models were established on a common basis of LTE [32,34,63,66,69,71,73,76,80,82,89,97-99] or partial-LTE [32,66,80,98,99]. Opinions diverge on how to frame nonequilibrium phenomena into the LTE scheme.

Use of an LTE-based model is feasible for characterizing the plasma with two parameters, i.e., temperature and electron number density, and therefore providing a basis for theory-experiment comparison. Unfortunately, most diagnostic works indicate that LTE does not exist throughout the ICP [32,63,66,69,71,89,97,99-101], rendering such a model inappropriate to mechanistic elucidation of analyte excitation.

An LTE-based model has two inherent drawbacks. First, it treats the portion of plasma under investigation as a closed system, whereas the real plasma is dynamic and open everywhere. In order to measure optical characteristics in the plasma, the plasma is considered as being closed because light absorption and emission is normally much faster than the dynamic flowing. In spatially resolved studies, however, the situation is completely different. When a particular point is considered as the chemical system of interest, the rest of the plasma constitutes the environment. So, there is an invisible boundary (a mathematical discontinuity) separating the system from its environment. If the detector is moved to another point observing a different portion of the plasma, the new position becomes the system of interest and the previous position is now part of the environment. Logically, no correlation should be found between these points otherwise they should be included in a single system defined by the same set of parameters, thus violating the basic assumption of localization of LTE.

Second, an assumption of steady state and/or equilibrium is automatically incorporated into an LTE-based model. This indicates that the vapor element under investigation must be homogeneous in temperature and concentration. A process such as diffusion, however, requires a concentration gradient within the system. Therefore, direct incorporation of diffusion with LTE is fundamentally self-contradictory. In other words, an LTE-based model is very specific and limiting but does provide considerable advantages in mathematical simplification and leaves very little room for modification.

An alternate approach to the equilibrium or steady state assumption is a dynamic one, in which all processes are considered kinetic ones which lead to time (or height) dependent distributions of analyte species. Theoretically, a precise elucidation of the system has to include distributions of all other species besides temperature and electron number density. This is, of course, too ambitious to be realistic. An idealized kinetic model treated by a stochastic approach is established.

Characteristic axial profiles of simulated and experimental distributions of analyte atoms and ions are compared. Two methods for rate constant evaluation are proposed. Detailed calculations of these constants will be given in the next chapter.

Theoretical Considerations

The Stochastic Approach

The optical signal indicated with a fixed detector is the integral signal resulted from every vapor element passing through the detector viewing zone during the time of integration. Usually, the analyte is introduced as tiny solution droplets which desolvate and vaporize into individual vapor plumes. The plumes expand as a function of height (time) and finally interdiffuse into a vapor continuum high in the tail of the plasma. If such an individual vapor plume is considered as a radiation source in the data acquisition process, the observed signal may be described as follows:

$$S(z,r) = C \sum_j n_j(z,r,d_0) \tag{2-1}$$

where $n_j(z,r,d_0)$ is the number density of an analyte species of interest for the jth element resulting from a droplet with initial diameter, d_0; z and r are the axial and radial coordinates of the viewing point with respect to the tip of the plasma aerosol tube (Fig. 1) and C is a constant. Since analytes are generally aspirated through the central channel of the plasma torch, analysis of any off-axis signal will require the information of flight pattern of the droplets. In addition, the plasma has already been proven to be very heterogeneous in the radial direction. Such an analysis is imagined to be very difficult. Moreover, the much simpler axial distribution should contain sufficient information for mechanistic interpretation of analyte atomization. So, only the axial distribution is considered in this work.

For simplicity, the argon flow is assumed to be laminar with a constant upward speed v, cm/s. The viewing location can then be specified with analyte flight time, which is the time an analyte species moves from the tip of aerosol tube upward to z position. If the nebulizer produces a great number of droplets with a size distribution, $P(d_0)$, then the summation in Eq. (2-1) can be described with an integration as

$$S(z) = C \int_0^\infty n(t',d_0)P(d_0)\delta d_0 \tag{2-2}$$

Fig. 1. A sketch diagram showing the different paths of migration of aerosol particles and their resultant vapor plumes in the central channel of an inductively coupled plasma.

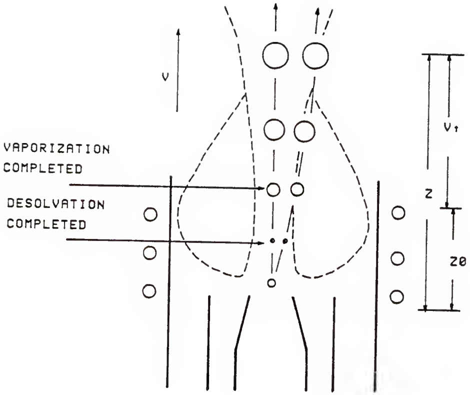
V
VAPORIZATION
COMPLETED
DESOLVATION
COMPLETED
V₁
Z
Z0

where $n(t',d_0)$ is the number density (cm^{-3}) of an analyte species produced from an initial droplet of diameter d_0 and at a time t'. Providing that the plasma is sufficiently reproducible, each droplet will nearly repeat the course of the preceding droplets of the same size. Each droplet undergoes desolvation, vaporization, atomization, ionization, etc., in approximately the same way at the same height (time).

Suppose that a droplet of interest completes desolvation and vaporization at the height z_0 above the tip of aerosol tube. From that height on, chemical reactions take place. Then, the time for these reactions will be $t = (z - z_0)/v$. The number density of an analyte species at location z can then be characterized by t and d_0 and may be expressed as

$$n(t,d_0) = p(t)n_0(d_0) \tag{2-3}$$

where $n_0(d_0)$ (or simply n_0) is the initial number density (cm^{-3}) of analyte species with vapor plume resulting from droplets of diameter, d_0, and p(t) is a function of time of reaction. Since n_0 is determined by the composition of the original droplet, once the composition is selected n_0 is fixed for a given d_0. The spatial (height) distribution of an analyte is, therefore, related to p(t) only.

If the droplets entering the plasma have a wide range of sizes, the spatial distribution of the resultant signals will be very difficult to predict. This is because droplets of different sizes experience different times of reaction. The integration in Eq. (2-2) is very complicated. Fortunately, most commercially available spray chambers are optimized to produce droplets of relatively uniform size. In this case, the axial signal profile can actually be approximated by p(t), the single droplet distribution. Consequently, a simulation of p(t) on the basis of a reasonable and manageable reaction scheme will reveal sufficient information about analyte atomization; an analysis of the spatially (height) resolved signal distribution, on the other hand, should allow direct estimation of reaction rate constants.

The Dynamic Model

The dynamic model proposed here is constructed on the basis of the following information:

(a) In a high-frequency ICP, the cooling effect of the aspirating argon stream as well as the skin effect of the eddy current result in the formation of a narrow channel which possesses a somewhat lower temperature than the annular induction region. The channel extends to the normal analytical zone. Major processes and reactions leading to analyte atomization and excitation occur in the channel.

(b) Under normal operational conditions, the residence time of analyte species in the channel is a few milliseconds [7,102].

(c) Spatially resolved studies [64,65,69,101,103-109] indicate that the electron number density, n_e, does not vary significantly in the channel.

(d) Generally speaking, temperatures in the ICP based on different degrees of freedom differ significantly, i.e., $T_e \geq T_{ion} > T_{ex} > T_{rot}$, indicating deviation from LTE. As to the axial distribution along the central channel, however, each temperature is nearly constant, at least over a suitable portion of the channel [65,79,101,105].

(e) It has been shown that the height where total decomposition of sample particles occurs depends critically upon the initial droplet sizes [102,108]. Vapor plumes from droplets of different sizes experience different times of reaction when they reach the observation zone. Therefore, control of a uniform size distribution is essential in both high precision analysis and diagnostic studies.

(f) It has been a general misbelief that observation of a constant signal is an indication of an equilibrium or steady state in the plasma. Actually, the signal consistency is merely the consequence of good reproducibility of the sample introduction system. Indeed, the possibility of equilibrium or a steady state should be treated only as limiting cases.

(g) A satisfactory model should generate a continuous function for analyte distribution over the entire region studied. For spatially resolved measurements, this consists of the entire portion of plasma under investigation. An LTE-based model is apparently inappropriate.

According to the above information, it is assumed that the central channel is a semi-infinite column of uniform temperature. (This does not exclude the fact that T_e, T_{ion}, T_{exc}, and T_{rot} may be different. It only requires that these temperatures be constant over the entire region of interest.) An analyte salt particle vaporizes completely when entering the column. Inside the column, all atomic, ionic, and molecular species are moving with the same translational velocity as the argon flow. The resultant vapor plume moves with the argon flow and expands on its way up.

To keep away from solving a set of complicated Fick's equations for all analyte species of interest, an approximation method is used where a set of moving coordinates located at the center of mass of the vapor plume is selected. With this approach, the diffusion problem is analogous to that of volume expansion under constant pressure.

The vapor plume from a single droplet can be realized as a slight perturbation to the central channel. It has intrinsically the same constituents as the plasma besides the molecular, atomic, and ionic species of analyte. Since the number densities of electrons, argon atoms, argon ions, etc. are assumed to be invariant in the column, analyte reactions involving collisions with these species can actually be treated as pseudo first-order reactions.

Solution of Rate Equations

A general reaction scheme is given in Fig. 2(A), where MX represents the gaseous molecular species, usually the metal oxide or hydroxide, when an aqueous sample is used; M and M^+ are the free atom and ion in the ground state, and M^* and M^{+*} are the excited atom and ion in the most populated excited states, respectively. All other excited states are not considered here for the obvious reason of simplicity. All rate constants are apparent constants consisting of

Fig. 2. Reaction schemes used for kinetic studies: (A) general scheme containing dissociation of a molecular species (usually metal oxide), ionization, recombination, and excitation of free atoms and ions; (B) simplified scheme consisting of possible rate-determining steps only. Volume expansion is also included.

(A)

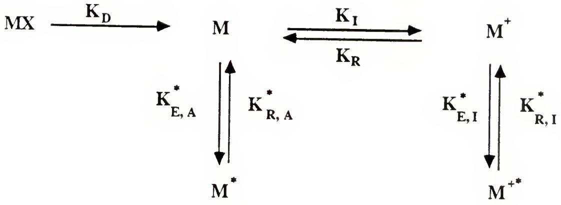
MX
K_D
M
K_I
K_R
M^+
K*_E, A
K*_R, A
K*_E, I
K*_R, I
M^*
M^+*

(B)

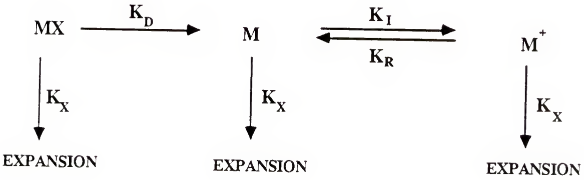
MX
K_D
M
K_I
K_R
M^+
K_X
K_X
K_X
EXPANSION
EXPANSION
EXPANSION

rate constants of many parallel reactions. For example, atomic excitation consists of the following possible reactions:

(i) Collisions with electrons

$$M + e^- \xrightarrow{k_1} M^* + e^-$$

(ii) Radiative recombination with ion-electron

$$M^+ + e^- \xrightarrow{k_2} M^* + h\nu$$

and $$M^{+*} + e^- \xrightarrow{k_3} M^* + h\nu$$

(iii) Three-body recombination with ion-electron

$$M^+ + 2e^- \xrightarrow{k_4} M^* + e^-$$

and $$M^+ + e^- + Ar \xrightarrow{k_5} M^* + Ar$$

(iv) Collisions with energetic argon

$$M + Ar^m \xrightarrow{k_6} M^* + Ar + h\nu,$$

$$M + Ar^m + e^- \xrightarrow{k_7} M^* + Ar + e^-$$

and $$M + Ar^m + Ar \xrightarrow{k_8} M^* + 2Ar$$

(v) Radiative excitation

$$M + h\nu \xrightarrow{k_9} M^*$$

The ionization processes include

(i) Penning ionization

$$M + Ar^m \xrightarrow{k_{10}} M^+ + e^- + Ar$$

(ii) Collisions with electrons

$$M + e^- \xrightarrow{k_{11}} M^+ + 2e^-$$

$$\text{and} \quad M^{+*} + e^- \xrightarrow{k_{12}} M^+ + e^-$$

(iii) Charge transfer reaction

$$M + Ar^+ \xrightarrow{k_{13}} M^+ + Ar$$

(iv) Radiative de-excitation

$$M^{+*} \xrightarrow{k_{14}} M^+ + h\nu$$

The excitation and ionization constants k_E^* and k_I are, respectively,

$$k_E^* = k_1 + k_2 + \dots + k_9$$

and

$$k_I = k_{10} + k_{11} + \dots + k_{14}$$

Since the residence time of the vapor plume in the channel is only a few milliseconds, reactions having significant influence on the analyte distribution must have rates of the order of $10^3\ s^{-1}$. Very fast and very slow reactions will have little kinetic significance. In other words, the characteristics of the analyte distributions are the result of those rate-determining reactions, and only these reaction kinetics can be regained from measurements of spatially resolved profiles.

Radiative transitions between atomic or ionic levels and population equilibration among states are several orders of magnitude faster than molecular dissociation, ionization, and recombination. Therefore, they are very unlikely to be the rate-determining steps. Steady state may be assumed for radiative transitions, but surely cannot be applied to the much slower reactions and processes.

If $M \rightleftharpoons M^*$ and $M^+ \rightleftharpoons M^{+*}$ are not the Rate Determining Steps (RDS), the reaction scheme can be further simplified as shown in Fig. 2(B). A set of rate equations can be written as follows:

$$dn_m/dt = -k_D n_m - n_m(d\ell n\ V/dt) \qquad (2\text{-}4)$$

$$dn_a/dt = k_D n_m - k_I n_a + k_R n_i - n_a(d\ell n\ V/dt) \qquad (2\text{-}5)$$

$$dn_i/dt = k_I n_a - k_R n_i - n_i(d\ell n\ V/dt) \qquad (2\text{-}6)$$

where n_m, n_a, and n_i represent the instantaneous number densities (cm^{-3}) of MX, M, and M^+, respectively. The term $d\ell n\ V/dt$ corresponds to the decrease in number density due to volume expansion of the vapor plume. Volume expansion is the result of diffusion and reactions giving rise to more product particles than the reactant particles and is a very complicated function of time. Fortunately, this term can be approximated with a contant, k_X, to an accuracy with actual experimental error (see Appendix A). This is reasonable because the relative change in volume, $d\ell n\ V/dt$, may be less significant than the direct change in volume, dV/dt. Furthermore, the vapor plume does not have a very well-defined boundary. Its volume can only be treated loosely as the most probable estimation. With the substitution of k_X, the rate equations can be expressed as follows:

$$dn_m/dt = -k_D n_m - k_X n_m \tag{2-7}$$

$$dn_a/dt = k_D n_m - k_I n_a + k_R n_i - k_X n_a \tag{2-8}$$

$$dn_i/dt = k_I n_a - k_R n_i - k_X n_i \tag{2-9}$$

Employing the Laplace transform, the above equations can be solved explicitly (see Appendix B for more detailed treatment). The time functions and their Laplace transforms are given below.

$$n_m = n_0 \exp(-at) \tag{2-10}$$

$$n_a = k_D n_0 \, [A \exp(-at) + B \exp(-bt) + C \exp(-ct)] \tag{2-11}$$

$$n_i = k_D k_I n_0 \, [D \exp(-at) + E \exp(-bt) + F \exp(-ct)] \tag{2-12}$$

$$\bar{n}_m = n_0/(s+a) \tag{2-13}$$

$$\bar{n}_a = k_D n_0 (s+d)/[(s+a)(s+b)(s+c)] \tag{2-14}$$

$$\bar{n}_i = k_D k_I n_0/[(s+a)(s+b)(s+c)] \tag{2-15}$$

where s is the Laplace parameter with respect to t and $\bar{n}_m$, $\bar{n}_a$, and $\bar{n}_i$ are the Laplace transforms of n_m, n_a, and n_i, respectively. The constants are

$$a = k_D + k_X \tag{2-16}$$

$$d = k_R + k_X \tag{2-17}$$

$$b = k_X \tag{2-18}$$

$$c = k_I + k_R + k_X \tag{2-19}$$

$$A = (d-a)/[(a-b)(a-c)] \tag{2-20}$$

$$B = (b-d)/[(a-b)(b-c)] \tag{2-21}$$

$$C = (d-c)/[(a-c)(b-c)] \tag{2-22}$$

$$D = 1/[(a-b)(a-c)] \tag{2-23}$$

$$E = -1/[(a-b)(b-c)] \tag{2-24}$$

$$F = 1/[(a-c)(b-c)] \tag{2-25}$$

As predicted, the number density of an analyte species can be specified by a droplet size dependent term, n_0, along with a kinetic dependent function. The latter consists of simple exponential functions of rate constants. Reactions with very large rate constants will automatically drop out of the scheme. Only those rate-determining steps (RDS) will have significant influences on the distribution.

Evaluation of Rate Constants

From Eqs. (2-10) to (2-15), rate constants can be evaluated by either of the two approaches which are discussed below.

(i) Curve Fitting Approach: The time (or height) distribution is seen to be the summation of several exponential components. A numerical fit of experimental data will provide a set of coefficients, A, B, C, D, E, F, a, b, c, and d. From these coefficients, the rate constants, k_D, k_I, k_R, and k_X can be estimated.

(ii) Statistical Moment Approach: A convenient relationship between the statistical moments and the Laplace transforms has been established [110]. The zeroth (S_0) and first (S_1) moments of n_m, n_a, and n_i can be easily obtained. The ionization constant, k_I, can be estimated directly from these moments. The expansion constant, k_X, may vary within a limited range. Rate constants k_D and k_R can be calculated using an educational guess of k_X.

Experimental

Although the plasma is in general relatively reproducible, temporal and local variations are expected to be unavoidable. To obtain high precision for rate constant estimation, it is desirable to have both (atomic and ionic) profiles acquired simultaneously along the same path in the plasma. Under this situation, even if there is a slight variation in the plasma, it will be displayed in both profiles and can be compensated for in the data processing step.

Figure 3 is a block diagram of the ICP spectrometer used in this study. The emission from the plasma central channel is focused onto the end of an ultraviolet-transmitting optical fiber (C) which is mounted on an optical bench (B_1). The fiber holder is mounted on a XYZ translation stage with the vertical translation driven by on HDM 12-480-4 stepping motor (E) and a digital drive system (I) (USM Corporation, Wakefield, MA) via a 5-cm micrometer (A) (L.S. Starrett Co., Athol, MA). The other end of the optical fiber is stationarily mounted on an optical bench (B_2). Radiation emerging from the fiber is collimated and split with a beam splitter (F) into two Heath (EU700) monochromators (D_1 and D_2) (Heath Co., Benton Harbor, MI). The photoelectrical signals from the two photomultiplier tubes are either traced with a two-pen chart recorder or digitized and sent to an IBM-personal computer (J) via a Stanford SR245 interface module (G) (Stanford Research, Inc., Palo Alto, CA).

Fig. 3. Block diagram of the ICP spectrometer.

(A) 5 cm micrometer, (B_1) and (B_2) optical fiber mount, (C) optical fiber, (D_1) and (D_2) Heath (EU 700) monochromator, (E) HDM 12-480-4 stepping motor, (F) beam splitter, (G) SR 245 interface module, (H) remote control, (I) USM digital drive system, and (J) IBM personal computer.

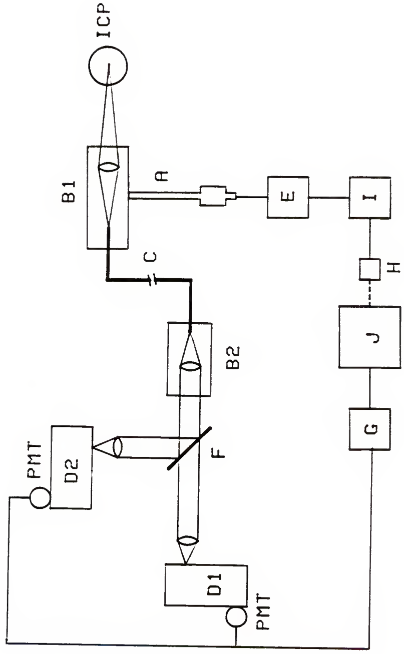
ICP
B1
A
E
I
C
H
J
B2
G
F
PMT
D2
D1
PMT

Metal solutions are prepared either from dilution of prepared atomic absorption standard solutions (Fisher Scientific Co., Fair Lawn, NJ) or from dissolution of reagent grade oxides or chlorides. For Ca and Mg, 50 ppm are used and for Y, 500 ppm is used.

Results and Discussion

Figures 4 and 5 show the atomic and ionic emission profiles of Ca and Mg. Three distinct characteristics have been examined by others but have not been satisfactorily interpreted; these are (1) the profiles are hump-shaped; (2) the atom and ion profiles peak at different positions with the ion peak always at higher heights; and (3) the ion line emission is more intense than the atom line emission.

To account for the hump shape, Horlick et al. [64,101] have substituted a linear temperature function into the Saha equation and have shown a direct correlation between the spatial behavior of the so-called "soft" atom line with the "normal temperature." The difficulty in this approach, as mentioned earlier, is that it essentially leads to the delocalization of LTE if a continuous analyte distribution function is required to cover the entire range of observation. In addition, new vertical (height) temperature profiles must be employed whenever an operational condition, such as rf power, argon flow rate, solution uptake rate, etc., is changed. Even if a good vertical temperature profile is calculated from a good

Fig. 4. Spatially resolved profiles of Ca atom and ion. The time scale corresponds to 0-30 mm in height above the load coil. The ion line emission should be normalized by multiplying a factor of 12.

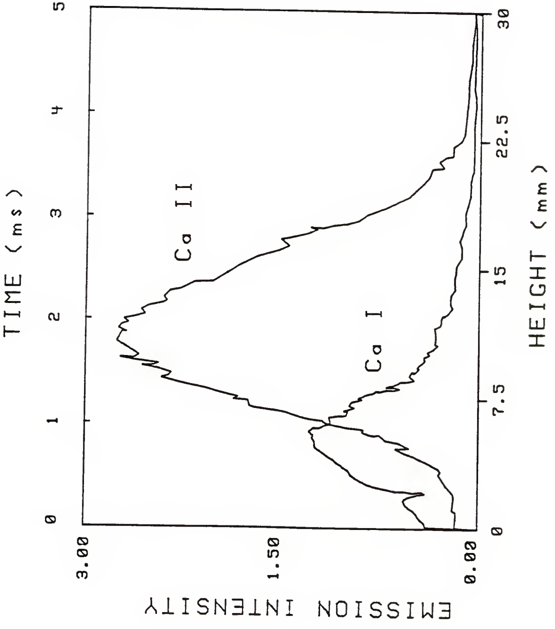
TIME (ms)
0
1
2
3
4
5
Ca II
Ca I
EMISSION INTENSITY
3.00
1.50
0.00
HEIGHT (mm)
0
7.5
15
22.5
30

Fig. 5. Spatially resolved profiles of Mg atom and ion. The time scale corresponds to 0-30 mm in height above the load coil. The ion line emission should be normalized by multiplying a factor of 9.2.

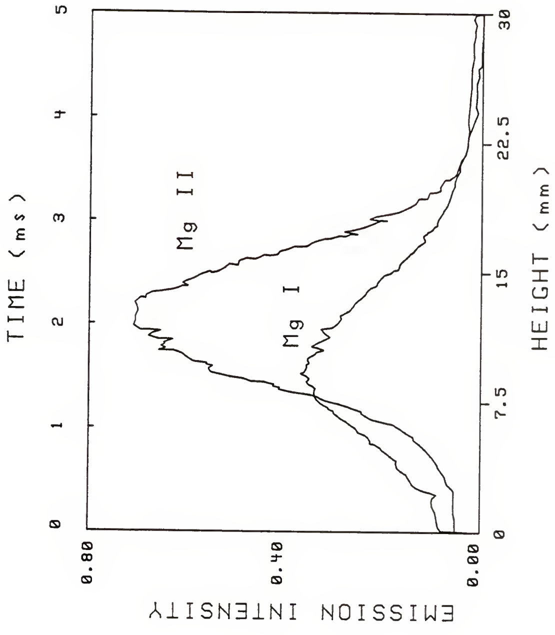
TIME (ms)
0
1
2
3
4
5
EMISSION INTENSITY
0.80
0.40
0.00
HEIGHT (mm)
0
7.5
15
22.5
30
Mg II
Mg I

set of data, little information about the analyte excitation mechanism can be retrieved.

The high ion/atom ratio is normally attributed to the so-called "suprathermal" effect excited by the metastable argon atoms in the plasma [66,69,71,111,112]. As pointed out by de Galan [79], such an argument is speculative because the lifetime of the metastable argon atom is much too short to be significant in supporting ionization well beyond the normal analytical zone. Hart et al. [113] have recently shown that the number density of the argon metastables is significantly suprathermal at the plasma center and even 10 mm above the coil if one assumes a temperature of 6500°K. However, at 20-25 mm above the coil, this overpopulation disappears and an equilibrium value for that temperature tends to be reached. Moreover, the referred temperature (6500°K) might not be appropriate for the argon excitation temperature. If one uses the values reported by Furuta [114] for the argon ionization temperature, which agree with those reported by Hart et al. [113], then the metastable levels are not overpopulated at all.

No satisfactory LTE explanation has yet been provided for the separation of atom and ion vertical spatial profiles. Models based on the Saha equilibrium imply that atomic and ionic vertical profiles should be similar in shape and peak position.

All of the above-mentioned problems can be demonstrated with the proposed dynamic model through the computer simulation (see Appendix C).

Both magnitude and shape of the spatial distribution are sensitive to choice of rate constants. Figure 6 shows a simulation of atom and ion distribution using a set of hypothetical rate constants of $k_D = 1\ ms^{-1}$, $k_I = 10\ ms^{-1}$, $k_R = 1\ ms^{-1}$, and $k_X = 1\ ms^{-1}$. The hump shape, the peak separation, and the high ion/atom ratios are clearly demonstrated. Figures 7-14 demonstrate the trends of change in the distribution induced by each of the four constants. An increase in k_D leads to both atom and ion profiles with increased amplitude and shifts of the peak maxima to lower heights in the plasma (Figs. 7 and 8). An increase in k_I shifts the maximum of atom profiles to the left together with a decrease in amplitude (Fig. 9). While in the ion profiles, the increase in k_I shifts the maximum to the left with an increase in amplitude (Fig. 10). An increase in k_R for atom profiles shifts the peak to the right with an increase in amplitude (Fig. 11). For the ion profiles, an increase in k_R shifts the peak maximum to the left with a decrease in amplitude (Fig. 12). An increase in k_X narrows the profiles of atom and ion, decreases the amplitude, and shifts the maximum to the left (Figs. 13 and 14). Experimentally, more than one process may often be affected by the change of an operational parameter. The distribution is the overall effect of the kinetic variations of these processes. For example, varying the rf power will cause both the decomposition and ionization to change drastically, whereas the volume expansion should be influenced little. Therefore, the change in signal profile will appear to

Fig. 6. Simulation of atom and ion distribution using a hypothetical set of rate constants of $k_D = 1\ \mathrm{ms}^{-1}$, $k_I = 10\ \mathrm{ms}^{-1}$, $k_R = 1\ \mathrm{ms}^{-1}$, and $k_X = 1\ \mathrm{ms}^{-1}$. The hump shape, the peak separation, and the high ion/atom ratios are clearly demonstrated.

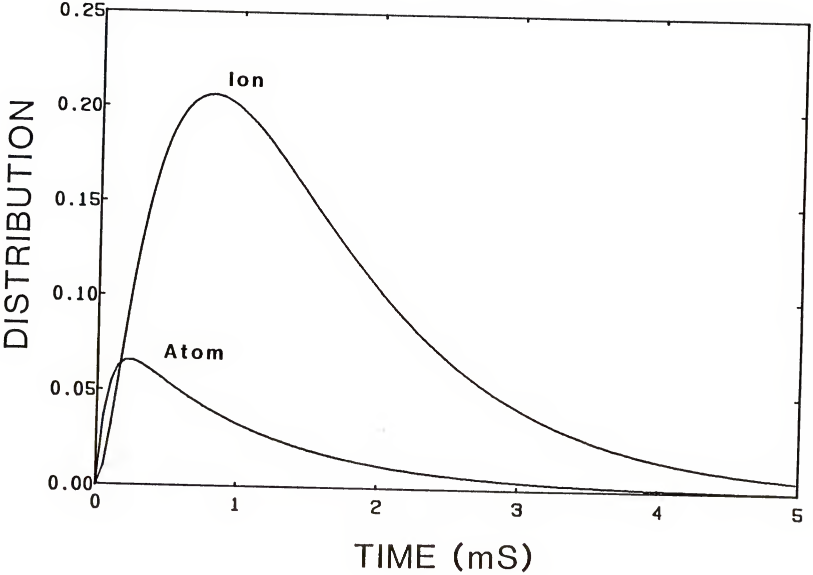
DISTRIBUTION
0.25
0.20
0.15
0.10
0.05
0.00
Ion
Atom
0
1
2
3
4
5
TIME (mS)

Fig. 7. Effect of k_D on the atom spatial (height) distribution. $k_I = 1\ ms^{-1}$, $k_R = 1\ ms^{-1}$, and $k_X = 1\ ms^{-1}$.

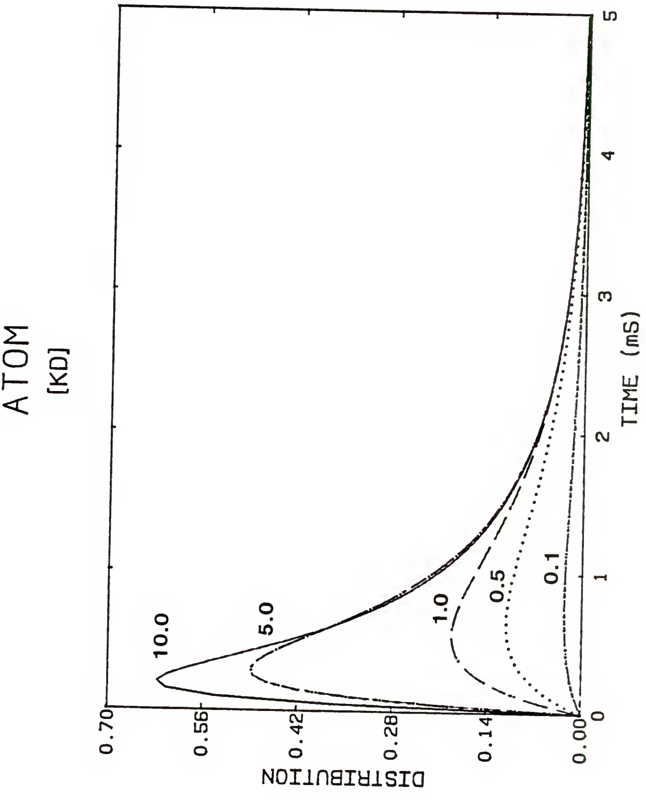
ATOM
[KD]
DISTRIBUTION
0.00
0.14
0.28
0.42
0.56
0.70
TIME (mS)
0
1
2
3
4
5
10.0
5.0
1.0
0.5
0.1

Fig. 8. Effect of k_D on the ion spatial (height) distribution. $k_I = 1\ ms^{-1}$, $k_R = 1\ ms^{-1}$, and $k_X = 1\ ms^{-1}$.

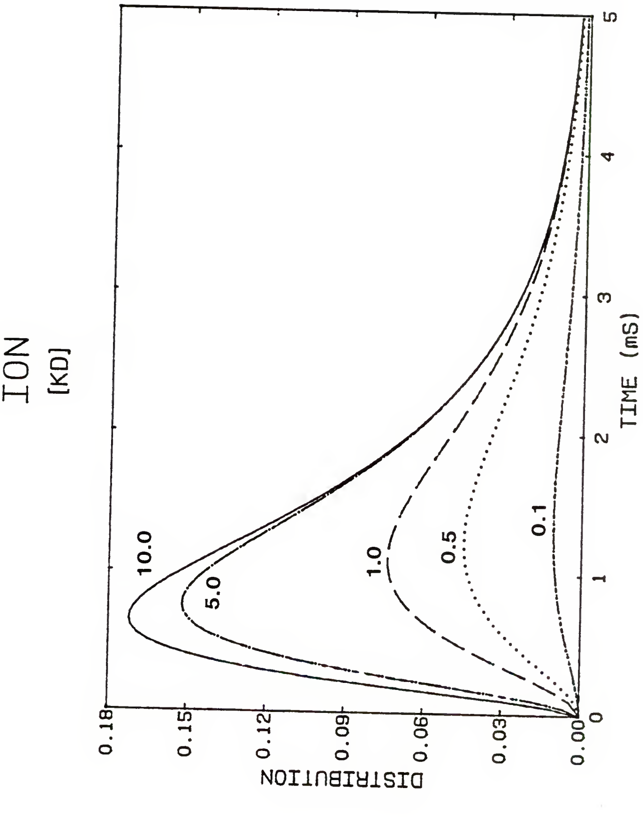
ION
[KD]
DISTRIBUTION
0.00
0.03
0.06
0.09
0.12
0.15
0.18
TIME (mS)
0
1
2
3
4
5
10.0
5.0
1.0
0.5
0.1

Fig. 9. Effect of k_I on the atom spatial (height) distribution. $k_D = 1\ \text{ms}^{-1}$, $k_R = 1\ \text{ms}^{-1}$, and $k_X = 1\ \text{ms}^{-1}$.

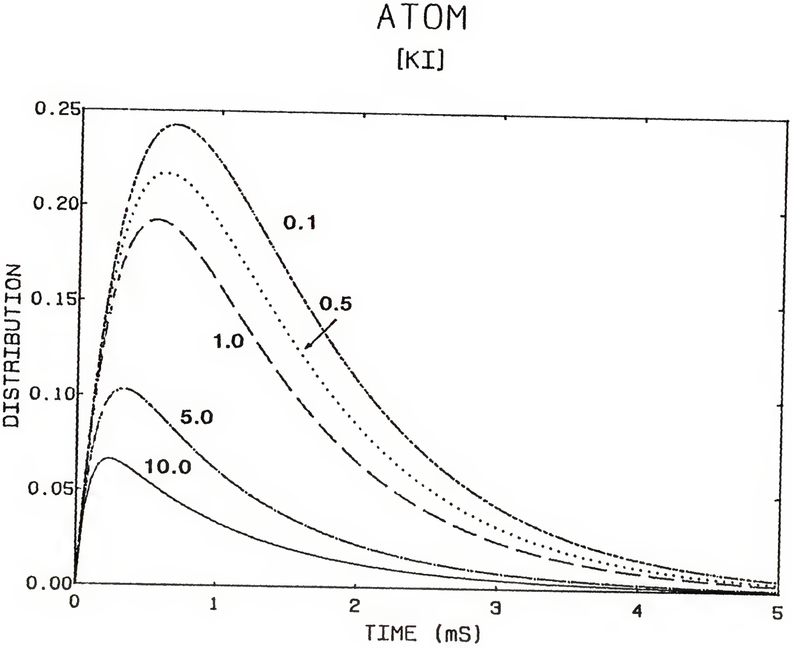
ATOM
[KI]
DISTRIBUTION
0.25
0.20
0.15
0.10
0.05
0.00
TIME (mS)
0
1
2
3
4
5
0.1
0.5
1.0
5.0
10.0

Fig. 10. Effect of k_I on the ion spatial (height) distribution. $k_D = 1\ \mathrm{ms}^{-1}$, $k_R = 1\ \mathrm{ms}^{-1}$, and $k_X = 1\ \mathrm{ms}^{-1}$.

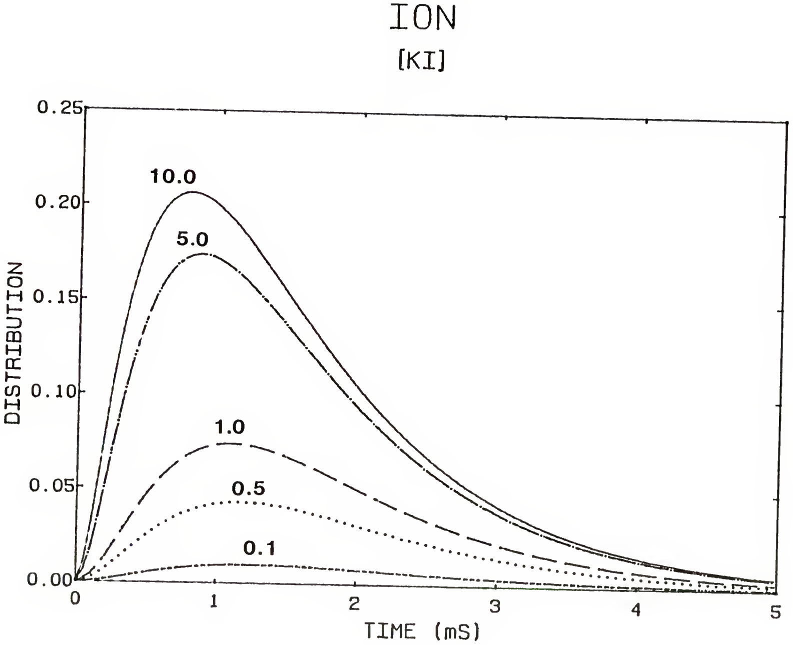
ION
[KI]
DISTRIBUTION
TIME (mS)
0.25
0.20
0.15
0.10
0.05
0.00
0
1
2
3
4
5
10.0
5.0
1.0
0.5
0.1

Fig. 11. Effect of k_R on the atom spatial (height) distribution. $k_D = 1\ \mathrm{ms}^{-1}$, $k_I = 1\ \mathrm{ms}^{-1}$, and $k_X = 1\ \mathrm{ms}^{-1}$.

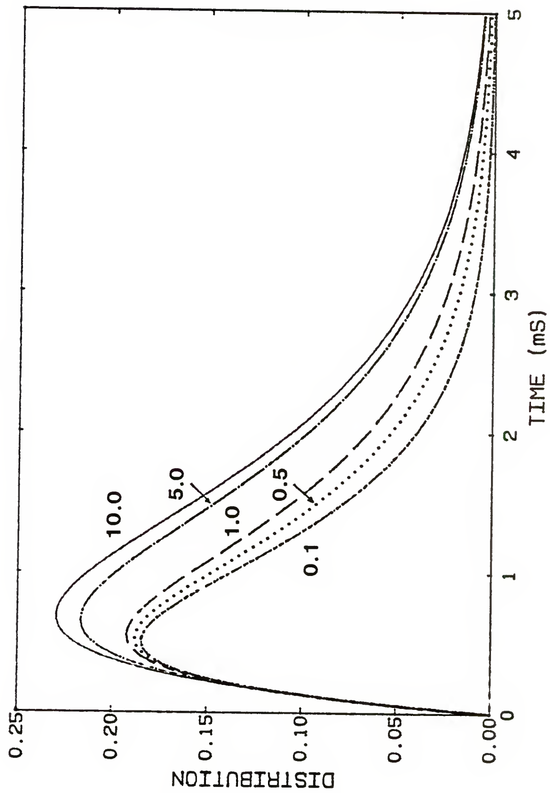

ATOM
[KR]

DISTRIBUTION
0.00
0.05
0.10
0.15
0.20
0.25
TIME (mS)
0
1
2
3
4
5
10.0
5.0
1.0
0.5
0.1

Fig. 12. Effect of k_R on the ion spatial (height) distribution. $k_D = 1\ \mathrm{ms}^{-1}$, $k_I = 1\ \mathrm{ms}^{-1}$, and $k_X = 1\ \mathrm{ms}^{-1}$.

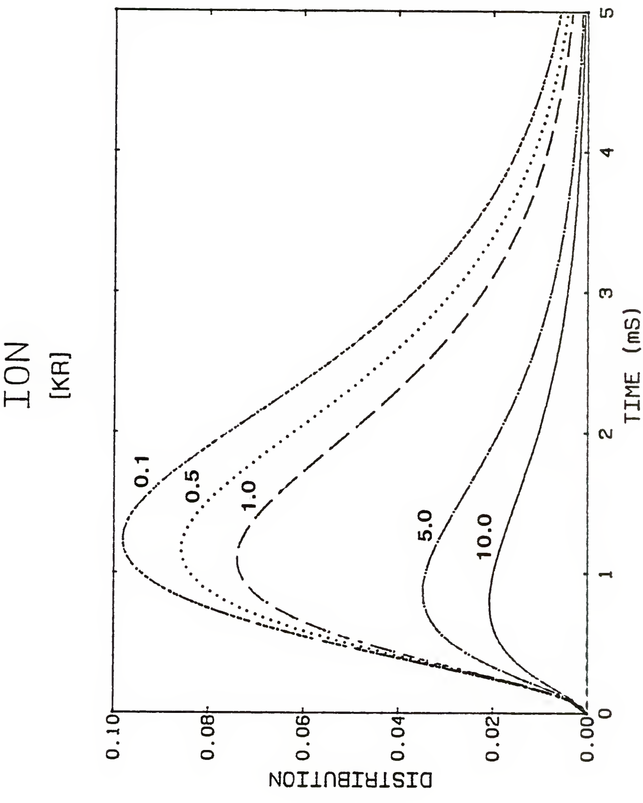
ION
[KR]
DISTRIBUTION
0.00
0.02
0.04
0.06
0.08
0.10
TIME (mS)
0
1
2
3
4
5
0.1
0.5
1.0
5.0
10.0

Fig. 13. Effect of k_X on the atom spatial (height) distribution. $k_D = 1$ ms^{-1}, $k_I = 1$ ms^{-1}, and $k_R = 1$ ms^{-1}.

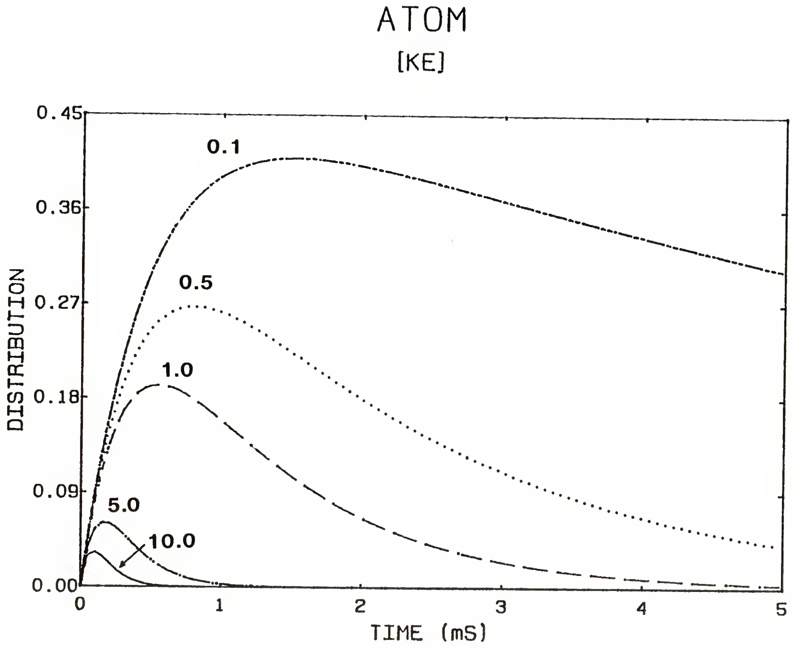
ATOM
[KE]
DISTRIBUTION
0.45
0.36
0.27
0.18
0.09
0.00
TIME (mS)
0
1
2
3
4
5
0.1
0.5
1.0
5.0
10.0

Fig. 14. Effect of k_X on the ion spatial (height) distribution. $k_D = 1$ ms^{-1}, $k_I = 1$ ms^{-1}, and $k_R = 1$ ms^{-1}.

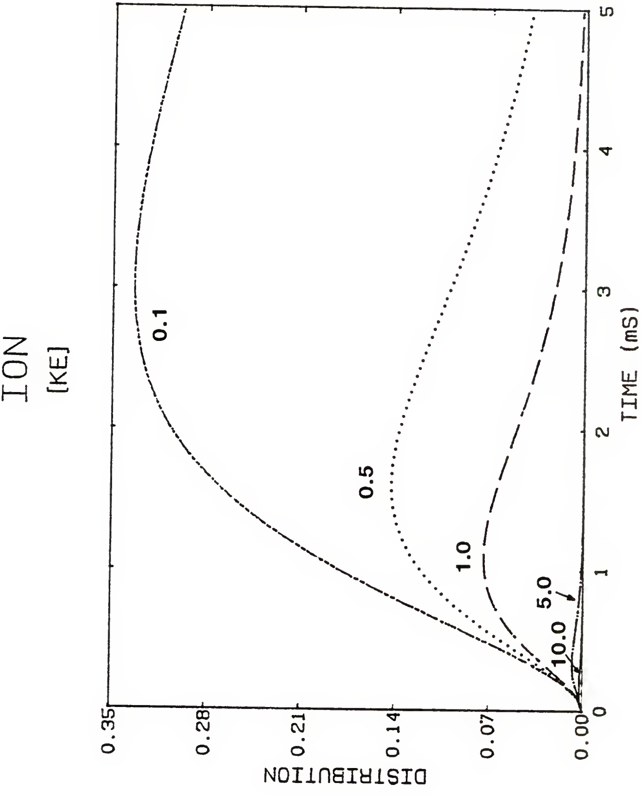
ION
[KE]
DISTRIBUTION
0.35
0.28
0.21
0.14
0.07
0.00
0
1
2
3
4
5
TIME (mS)
0.1
0.5
1.0
5.0
10.0

follow the dominating process. The profiles shown in Fig. 15 are Ca atom emission obtained by varying rf power. It is seen that the vertical emission profile peaks at a lower height with increasing amplitude as the rf power is increased. This trend is similar to that of increasing the decomposition rate constant, k_D, but opposite to that of increasing k_I, the ionization constant. So, in this case, it is conceivable that an increase in rf power affects the decomposition of Ca molecular species more than the ionization of the free Ca atom. If the molecular species is mainly CaO which has bond strength $D°$ (298°K) of about 462.8 KJ/mol (4.80 eV) [115] comparable to the Ca ionization potential of 6.113 eV, the change in rf power will, of course, affect the decomposition more than the ionization process.

The existence of metal oxide species in the plasma can be demonstrated by the molecular emission of yttrium (Fig. 16). The sharp decrease in intensity of the YO band at the lower heights indicates rapid decomposition with height. The small hump appearing higher in the tail plasma may be attributed to the recombination of free Y atoms with entrained atmospheric oxygen atoms. A more detailed examination will be studied in the future.

Fig. 15. Calcium atom emission profiles at various rf power.

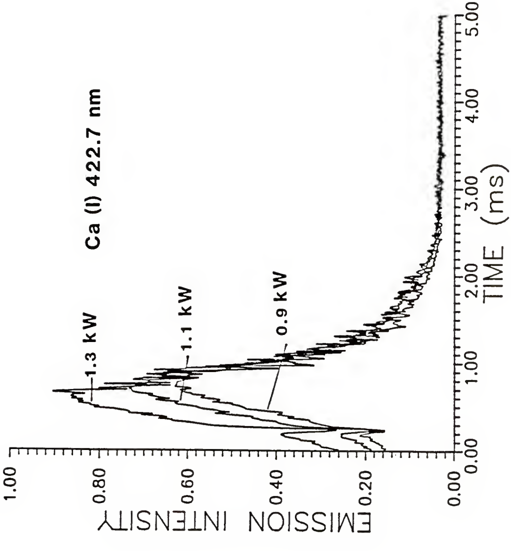
Ca (I) 422.7 nm
1.3 kW
1.1 kW
0.9 kW
EMISSION INTENSITY
0.00
0.20
0.40
0.60
0.80
1.00
TIME (ms)
0.00
1.00
2.00
3.00
4.00
5.00

Fig. 16. Emission profiles of YO band (597.2 nm) and Y(II) line (371.0 nm). The full scale for the YO emission was 0.01 V, whereas that for Y(II) line was 10 V.

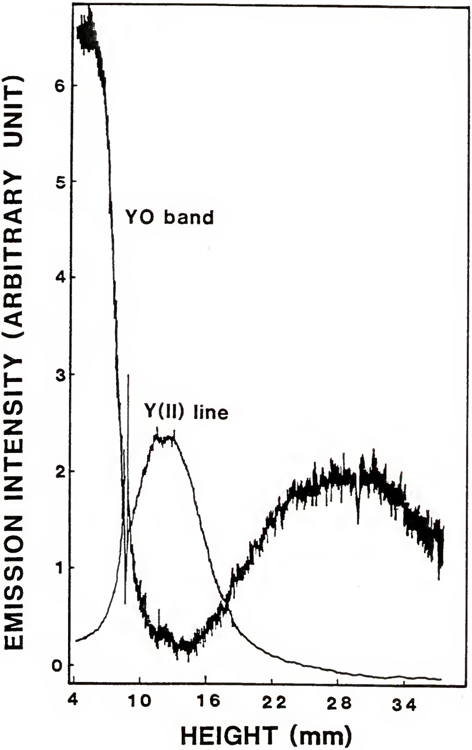
YO band
Y(II) line
EMISSION INTENSITY (ARBITRARY UNIT)
HEIGHT (mm)
0
1
2
3
4
5
6
4
10
16
22
28
34

CHAPTER 3

ESTIMATION OF RATE CONSTANTS USING STATISTICAL MOMENTS OF SPATIALLY RESOLVED SIGNAL PROFILES FOR THE ELUCIDATION OF ANALYTE ATOMIZATION MECHANISMS IN AN INDUCTIVELY COUPLED PLASMA

Introduction

During its residence in a plasma, an analyte species undergoes many chemical and physical transitions through exchange of energy with other species in its vicinity. As a result, the analyte is in different forms or states at different locations. When a great number of particles containing analyte is introduced continuously and reproducibly, a spatial distribution of these forms (molecular, atomic, and ionic) is established. Using space resolved spectrometry techniques, the distribution of some of these analyte forms can be individually probed. The resultant height resolved signal profiles contain kinetic information about the chemical and physical processes which lead to the specific distribution. Most of the previous space-resolved studies ignored the kinetic aspect and the plasma is treated as a closed system at LTE or at steady state. This assumption oversimplifies the complexity of the plasma and has led to many controversial conclusions.

A dynamic approach to interpret the mechanism of atomization of analyte species has been established in Chapter 2. It focused on the analyte distribution resulting from a single solution droplet.

Using basic concepts of plasma physics and chemistry, it is explicitly formulated the axial distribution functions for the molecular, atomic, and ionic analyte species.

Statistics is very often concerned with the distribution curves expressing the frequency (or probability) of some phenomenon. Many of these curves can be expressed by means of the Gauss, the Poisson, or the binomial distribution curve. Some distribution curves, however, cannot be characterized by any of the known distributions, and in this case statistics resort to expressing the distribution by means of a series of terms, which contain some known distribution function, e.g., that of Gauss, while being corrected by terms that are functions of the so-called statistical moments.

The spatially resolved signal profile is a typical distribution curve or probability density curve which describes the frequency of the elements of the set, i.e., the concentration as the number of particles in a certain volume, having a corresponding property, i.e., the spatial position, as it depends upon the quantity of the property, the time. This signal profile, which is also employed to represent the concentration curve as a function of time at a fixed height in the plasma, can be well characterized by the statistical moments.

In this chapter, the estimation of rate constants through the zeroth and first moments of the height-resolved emission profiles will be introduced in detail.

Theoretical Considerations

In the previous chapter, the following reaction scheme was used to estimate analyte distribution:

$$MX \xrightarrow{k_D} M \underset{k_R}{\overset{k_I}{\rightleftharpoons}} M^+ \qquad (3\text{-}1)$$

where MX, M, and M^+ are the molecular, free atomic, and single-charged ionic species; and k_D, k_I, and k_R are rate constants for decomposition (atomization), ionization, and recombination, respectively. The population equilibrations among atomic levels and among ionic levels are considered much too fast to be the rate-determining steps. A fourth rate constant, k_X, is introduced to take into account the volume expansion of the vapor plume from the solution droplet under investigation.

Application of Laplace transform to the rate equations of the above reaction scheme gives the number densities of MX, M, and M^+ in the Laplacian domain designated as $\bar{n}_m$, $\bar{n}_a$, and $\bar{n}_i$, respectively. These are

$$\bar{n}_m = n_0/(s+a) \qquad (3\text{-}2)$$

$$\bar{n}_a = k_D n_0 (s+d)/[(s+a)(s+b)(s+c)] \qquad (3\text{-}3)$$

and

$$\bar{n}_i = k_D k_I n_0/[(s+a)(s+b)(s+c)] \qquad (3\text{-}4)$$

where s is the Laplace variable with respect to the interaction time,

t. The constants are

$$a = k_D + k_X \tag{3-5}$$

$$d = k_R + k_X \tag{3-6}$$

$$b = k_X \tag{3-7}$$

$$c = k_I + k_R + k_X = k_I + d \tag{3-8}$$

and n_0 is the initial number density of the molecular species in the solution droplet under investigation.

Any distribution function, C(t), can be characterized by its statistical moments:

$$S_j = \int_0^\infty t^j C(t)dt, \qquad j = 0,\ 1,\ 2,\ \ldots \tag{3-9}$$

or its normalized moments:

$$\bar{S}_j = S_j/S_0 = \int_0^\infty t^j C(t)dt/\int_0^\infty C(t)dt \tag{3-10}$$

The zeroth moment, S_0, defines the area under the distribution profile, and $\bar{S}_1$ defines the center of gravity of the profile. If the distribution is symmetrical with respect to t, $\bar{S}_1$ will coincide with the profile maximum. For moments higher than the first moment, it is more convenient to calculate them around S_1. They are usually called the central moments:

$$\tilde{S}_j = \int_0^\infty (t-\bar{S}_1)^j C(t)dt / \int_0^\infty C(t)dt, \qquad j = 2, 3, \ldots \qquad (3\text{-}11)$$

The second central moment, $\tilde{S}_2$, is seen to be the difference of $\bar{S}_2$ and the square of $\tilde{S}_1$ (it is the variance of the distribution and is a measure of the profile width); $\tilde{S}_3$ and all higher odd moments furnish information on the asymmetry of the profile; $\tilde{S}_4$ and other even moments measure the peak flattening; and $\tilde{S}_3$ and $\tilde{S}_4$ are usually related to the skew and excess of the profile:

$$s = \tilde{S}_3 / \tilde{S}_2^{3/2} \qquad (3\text{-}12)$$

and

$$e = (\tilde{S}_4 / \tilde{S}_2^{\,2}) - 3 \qquad (3\text{-}13)$$

These quantities (s and e) are measures of deviation from a Gaussian peak.

The distribution function, C(t), of a kinetic system consists of rate constant of all rate-determining steps. Accordingly, its statistical moments are functions of these rate constants. Theoretically, one can solve these functions simultaneously for any number of the rate constants. However, because of the complexity of these functions, the solution may not be readily obtainable. It is, therefore, advisable to keep the number of steps (see equation) to the lowest possible in the reaction scheme so that only moments of the lower orders are necessary.

Yamaoka and Nakagawa [116], Cutter [117], and McQuarrie [118] have developed a convenient relationship between the statistical moments and the Laplace transform. Chan et al. [110] have used such an approach for rate constant estimation in several simple kinetic systems, such as hydrolysis of spirohydantoin mustard and diaziquone. The relationship is given as follows:

$$S_0 = \int_0^\infty C(t)dt = \lim_{s\to 0} \int_0^\infty e^{-st}C(t)dt = \lim_{s\to 0} \bar{C} \qquad (3\text{-}14)$$

and for higher moments,

$$S_j = \lim_{s\to 0}[(-1)^j \int_0^\infty t^j e^{-st}C(t)dt] = \lim_{s\to 0}[(-1)^j d^j\bar{C}/ds^j] \qquad (3\text{-}15)$$

where $\bar{C}$ is the Laplace transform of the distribution function C(t).

Applying the above operation to Eqs. (3-3) and (3-4), one obtains the zeroth and first moments for the free atom and the singly charged ion of the analyte:

$$(S_0)_a = k_D n_0 d/abc \qquad (3\text{-}16)$$

$$(S_0)_i = k_I k_D n_0/abc \qquad (3\text{-}17)$$

$$(S_1)_a = (S_0)_a[1/a + 1/b + 1/c - 1/d] \qquad (3\text{-}18)$$

and

$$(S_1)_i = (S_0)_i[1/a + 1/b + 1/c] \qquad (3\text{-}19)$$

The subscripts inside the bracket represent the order of the moments, whereas those outside the bracket represent the analyte species, and a for free atom and i for the singly charged ion. Combination of Eqs. (3-18) and (3-19) gives

$$d = 1/[(\bar{S}_1)_i - (\bar{S}_1)_a] \qquad (3\text{-}20)$$

The ratio of Eqs. (3-16) and (3-17) gives

$$k_I = d(S_0)_i/(S_0)_a \qquad (3\text{-}21)$$

Substitution of Eqs. (3-20) and (3-21) into Eq. (3-8) yields

$$c = d[(S_0)_i/(S_0)_a + 1] \qquad (3\text{-}22)$$

Rearrangement of Eq. (3-19) gives

$$1/a + 1/b = (\bar{S}_1)_i - 1/c = w \qquad (3\text{-}23)$$

Combination of Eqs. (3-5) and (3-23) gives

$$k_D = b(2-wb)/(wb-1) = k_X(2-wk_X)/(wk_X-1) \qquad (3\text{-}24)$$

Unfortunately, in the present case, the second and higher statistical moments provide no additional information for the explicit solution of a and b. Furthermore, molecular emission for most elements is either very small or nondetectable, making the evaluation of n_0 extremely difficult. Therefore, constants a and b can only be estimated iteratively.

As discussed in Appendix A and as indicated in Eq. (3-24), k_D and k_X do not vary independently. The constant k_D can be any value but k_X is bound in the very narrow range between 1/w and 2/w. Within the "more or less" stabilized central plasma channel, the rate of vapor plume expansion is relatively constant.

The dimensionless factor, $wk_X = 1 + \frac{k_X}{k_D+k_X}$, indicates the relative contribution of molecular dissociation and vapor plume expansion to the overall atomization process, i.e., $100(wk_X-1)$ percent is attributed to plume expansion and $100(2-wk_X)$ percent to decomposition.

Experimental

Instrumental Set-Up

The detailed system has been described in Chapter 2. The emission from the plasma axial channel is focused on one end of an optical fiber which is driven vertically with a stepping motor. Radiation leaving the other end of the fiber is collimated and split into two Heath monochromators set at different wavelengths. With this setup, the atomic and ionic emission from any point in the plasma are measured simultaneously.

Method of Calculation

The two optical channels do not have identical sensitivities. Before any processing of data, each signal profile is corrected for background emission and normalized such that both atom and ion profiles are compared under identical sensitivity conditions.

The software of the SR 245 module has a built-in integration program which is convenient for direct calculation of the zeroth moment from the calibrated signal profile. For calculation of higher moments, the signal intensity registered in each bin is multiplied by an appropriate power of its bin number to generate a new profile before integration is performed (see Appendix D). Since the bin number is directly related to the height in the plasma, which is, in turn, related to the time of reaction, this manipulation is the same as integrating the function $t^nC(t)$, with $n = 1, 2, \ldots$. The resulting statistical moments are then fed into another program for rate constant evaluation (see Appendix E).

As discussed above, k_D and k_X are interrelated through Eq. (3-24) with k_X varying in a very narrow range between 1/w and 2/w. For a very fast dissociation, k_X has a value very close to 1/w, whereas k_X approaches 2/w, as k_D approaches zero. Thus, based on the bond strength of MO, one can make an educated guess of k_X. Substitution of this value into Eq. (3-24) gives the corresponding value of k_D. The constant k_R is then calculated from Eq. (3-6). With this set of rate constants, the atomic and ionic signal profiles can be simulated. If the shape of these profiles does not match with the experimental ones, another guess of k_X is made. This process is repeated until a reasonably good match is reached. Since k_I is directly obtained from experimental signal profiles, the other rate constants so obtained can certainly be considered as reliable estimates. The impact of variation in experimental conditions, such as rf power, addition of interfering species, argon gas flow rate, solution uptake rate, etc., can now be quantitatively studied through investigation of the change in the four rate constants.

Operational Conditions

The plasma is maintained with an argon flow rate of 15 LPM together with an aspiration rate of 0.48 LPM. The moving end of the optical fiber covered a distance of about 3.0 cm in 25,000 steps; approximately 1400 data points are registered in one scan. The scan can be either in the upward or downward direction. The reproducibility of the stepping motor is very good. It returns to the same starting point each time. The stepping motor is mounted on an aluminum block which is a heat sink. The block can slide back and forth easily to release tension in the coupling cable such that a constant torque is applied to uniformly drive the micrometer.

Results and Discussion

The emission signal is registered in binary code with the SR 265 module. It is later transformed to ASCII code for plotting with a grapher software package (see Appendix F) (GRAPHER, Golden Software, Inc., Golden, CO). Figures 17 through 20 are a few examples of these reconstructional plots. For the sake of saving computer memory and computation time, only every fifth data point is transformed and plotted.

The linear argon flow rate is not directly measured in this study. It is estimated using the argon volume flow rates, the torch

Fig. 17. Calcium atom emission profiles at various rf power.

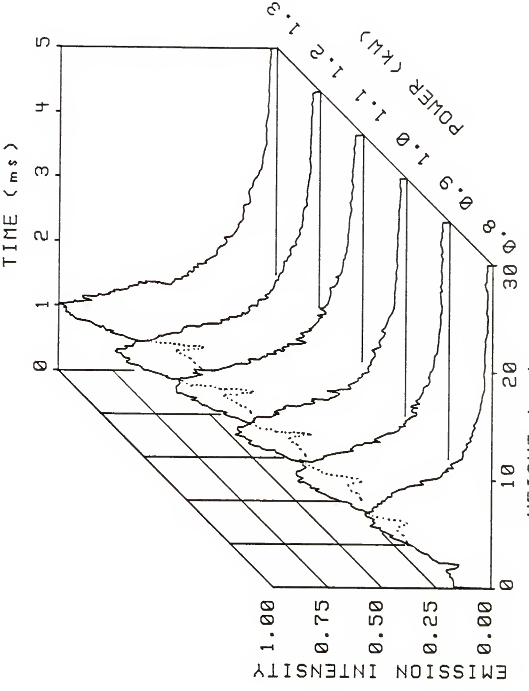
TIME (ms)
0
1
2
3
4
5
POWER (kW)
0.8
0.9
1.0
1.1
1.2
1.3
HEIGHT (mm)
0
10
20
30
EMISSION INTENSITY
0.00
0.25
0.50
0.75
1.00

Fig. 18. Magnesium atom emission profiles at various rf power.

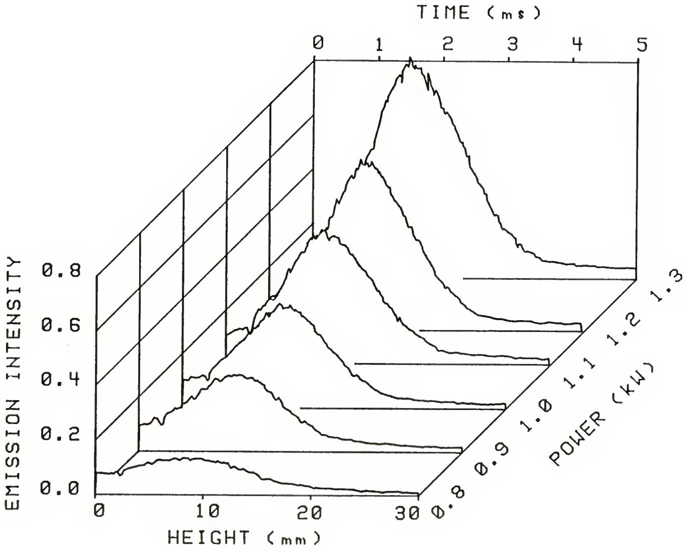
TIME (ms)
0
1
2
3
4
5
EMISSION INTENSITY
0.0
0.2
0.4
0.6
0.8
HEIGHT (mm)
0
10
20
30
POWER (kW)
0.8
0.9
1.0
1.1
1.2
1.3

Fig. 19. Calcium ion emission profiles at various rf power.

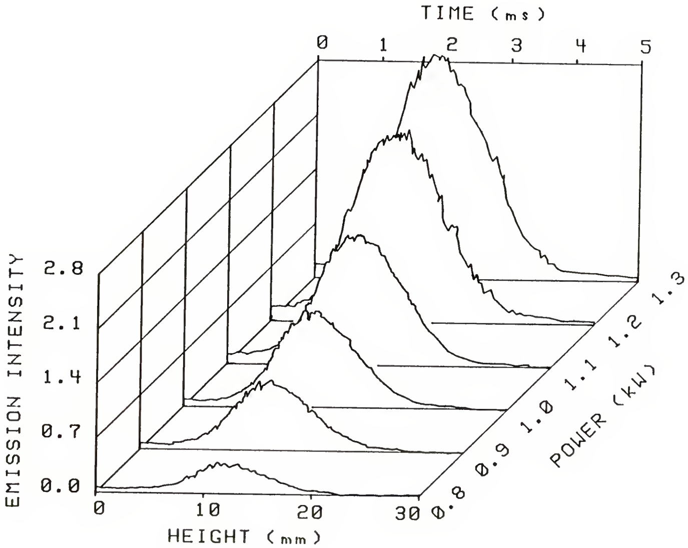
TIME (ms)
0
1
2
3
4
5
EMISSION INTENSITY
2.8
2.1
1.4
0.7
0.0
0
10
20
30
HEIGHT (mm)
0.8
0.9
1.0
1.1
1.2
1.3
POWER (kW)

Fig. 20. Magnesium ion emission profiles at various rf power.

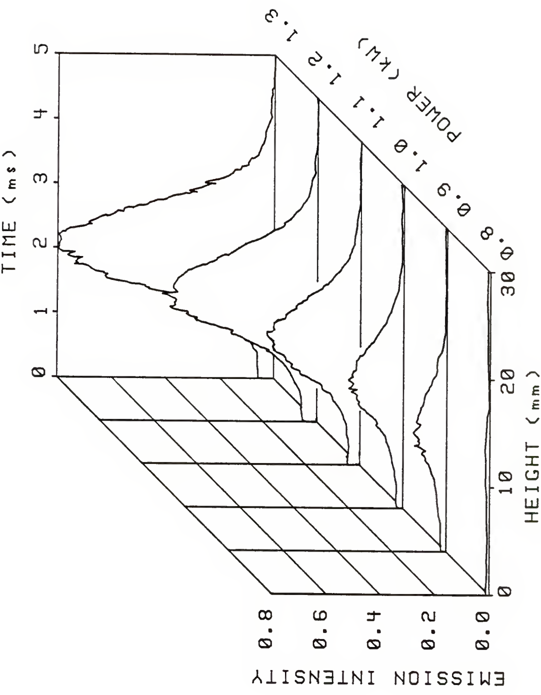
TIME (ms)
0
1
2
3
4
5
POWER (kW)
0.8
0.9
1.0
1.1
1.2
1.3
HEIGHT (mm)
0
10
20
30
EMISSION INTENSITY
0.0
0.2
0.4
0.6
0.8

tube diameter, and an estimated temperature of 5000°K. However, both the plasma temperature and the plasma size may vary with rf power and argon flow velocity in the central channel may not be the same as that in the perimeter region because argon is introduced through different tubes. The linear argon velocity in the central channel is more likely to be overestimated if the total flow rate is used in the calculation. Because an accurate velocity measuring device was not available, it was convenient to take 5 ms as the average residence time for all analyte particles in the portion of the channel under investigation. This estimation may be a little too large, but variation in the rate dependent distributions should not be affected.

All profiles (Figs. 17-20) are hump-shaped with the atom peak coming earlier than the ion peak, and the ion line emission is more intense than the atom line. The peak shape variation with respect to the rf power is shown in Figs. 17 and 18 for free Ca and Mg atoms and in Figs. 19 and 20 for their corresponding ions. The shift in peak maximum toward shorter time (lower height) with increase in rf power is clearly demonstrated in Ca atom emission but is nearly invariant for Mg atom emission. The peak position in both ion emission profiles is not affected by increase in rf power.

As indicated in Eq. (3-21), the ionization constant, k_I, is directly related to the product of d and $(S_0)_i/(S_0)_a$. The parameter d is a measure of the peak separation of the atom and ion profiles, and $(S_0)_i/(S_0)_a$ is the overall ion-to-atom ratio within the channel under study. Since the first moment of the ion profile is seen to be nearly independent of the rf power, d actually reflects the shift of the atom profile with rf power. The greater the shift in the atom profile, the smaller the parameter d will be. On the other hand, an increase in rf power normally increases the ion-to-atom ratio. If these two possible factors cancel each other, such as in the Mg case, the ionization constant, k_I, is apparently power independent. Otherwise, k_I will be power sensitive, as in the Ca case, where the dependence appears to be linear (Fig. 21).

The estimation of k_X, k_R, and k_D is not as straight-forward as the estimation of k_I as indicated in the theoretical section. Fortunately, the variation in k_X is very narrow; its value is limited mainly by the first moment of the ion profile (see Eqs. 3-22 and 3-23). For $(S_1)_i$ = 2 ms, corresponding to a height of 1.2 cm above the load coil, the value of k_X is bound between 0.5 to 1.0 ms^{-1}. At the middle point, equivalent to $k_Xw = 1.5$, k_X and k_D are numerically identical. Below this point, k_D increases sharply as k_X decreases (Fig. 22). This region corresponds to rapid dissociation of molecular analyte species and is applicable to elements with low M-O bond strength or to operation in the high rf power region. The slow decrease in k_D vs k_X in the high k_Xw region, on the other hand, corresponds to operation in the low rf power region.

Because k_X varies only within a very narrow range, we have used several approaches to estimate its value. First, we assumed it is independent of the rf power and assigned it a value according to the analyte M-O bond strength. The stronger the M-O bond, the greater

Fig. 21. Variation of ionization rate constants, k_I, of Ca and Mg with rf power.

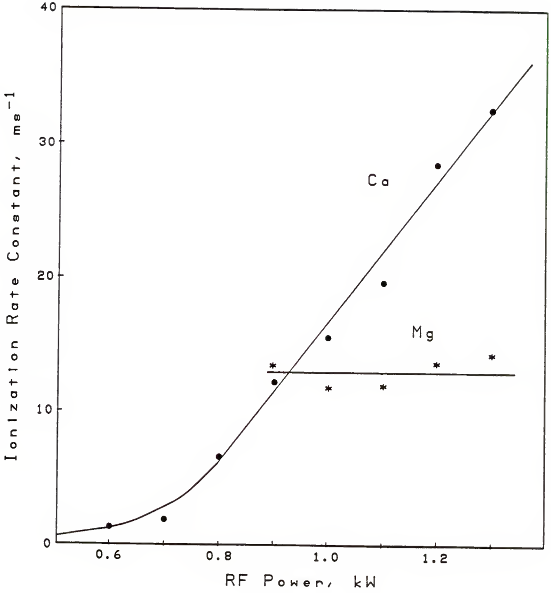
40
30
20
10
0
0.6
0.8
1.0
1.2
RF Power, kW
Ionization Rate Constant, ms^{-1}
Ca
Mg

Fig. 22. Variation of k_D/k_X with $k_X w$.

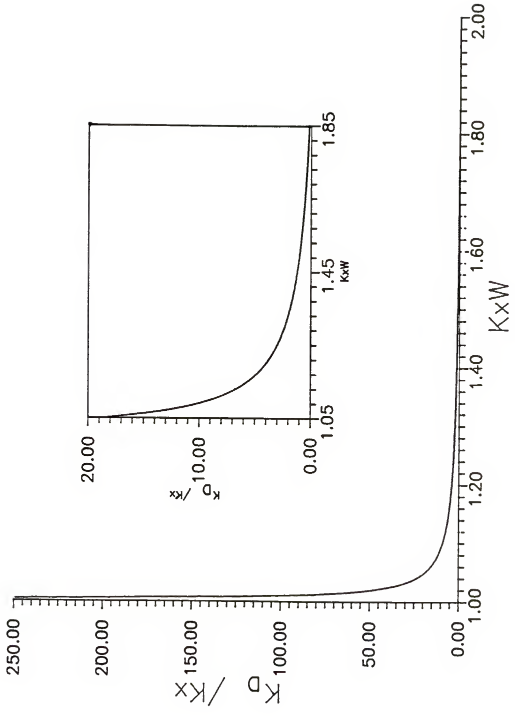

K D /Kx
250.00
200.00
150.00
100.00
50.00
0.00
1.00
1.20
1.40
1.60
1.80
2.00
KxW
K D /Kx
20.00
10.00
0.00
1.05
1.45
1.85
KxW

k_X will be resulting in a smaller k_D. Second, we assigned a constant k_Xw for each analyte to account for the slight power dependence of k_X. However, none of these approaches gave satisfactory simulations. A third option was taken by assuming a linear dependence of k_Xw on the rf power (see Table 1). This implies that k_D increases along the curve shown in Fig. 21 as rf power is increased. The linearly assumption is based on the apparent linear dependence of k_I of Ca on the rf power (Fig. 21).

Calcium has a higher M-O bond strength and a lower ionization potential than magnesium. Therefore calcium oxide will be more difficult to dissociate and calcium ions will readily recombine with electrons, i.e., a lower k_D and a higher k_R for Ca than Mg. Using this information, we assume that k_Xw for Ca varies linearly from 1.85 to 1.15 as the rf power increases from 0.6 to 1.30 kW. The calculated rate constants (see Table 1) are then used for simulation. The trends in the variation of profile characteristics are seen to be quite agreeable with the experimental trends. The peak separation, the high ion/atom ratio, the shift of the atom profile, and the enhancement of peak amplitude on the rf power are clearly demonstrated in Figs. 23-25. Similar theory-experiment agreements are also observed for magnesium.

Even though it is generally accepted that the ICP is not in local thermal equilibrium, the Saha equilibrium between total ion (n_i) and atom (n_a) concentrations is still commonly believed to hold. The Saha equation is

Table 1. Rate Constants Estimated From Ca Atom and Ion Line Signal Profiles.

rf Power (kW)	k_I (ms^{-1})	k_D (ms^{-1})	k_R (ms^{-1})	k_X (ms^{-1})	$k_X W$
1.30*	32.57	3.28	0.84	0.58	1.15
1.20	28.40	1.53	0.78	0.65	1.25
1.10*	19.77	1.21	0.81	0.65	1.35
1.00	15.58	0.87	0.80	0.71	1.45
0.90*	12.20	0.63	0.79	0.77	1.55
0.80	6.62	0.45	0.79	0.84	1.65
0.70	1.92	0.30	0.53	0.91	1.75
0.60	1.36	0.16	0.22	0.90	1.85

* Rate constants used for simulation shown in Figs. 23-25.

Fig. 23. Simulation of Ca atom and ion distribution using $k_I = 32.57\ ms^{-1}$, $k_D = 3.28\ ms^{-1}$, $k_R = 0.84\ ms^{-1}$, and $k_X = 0.58\ ms^{-1}$.

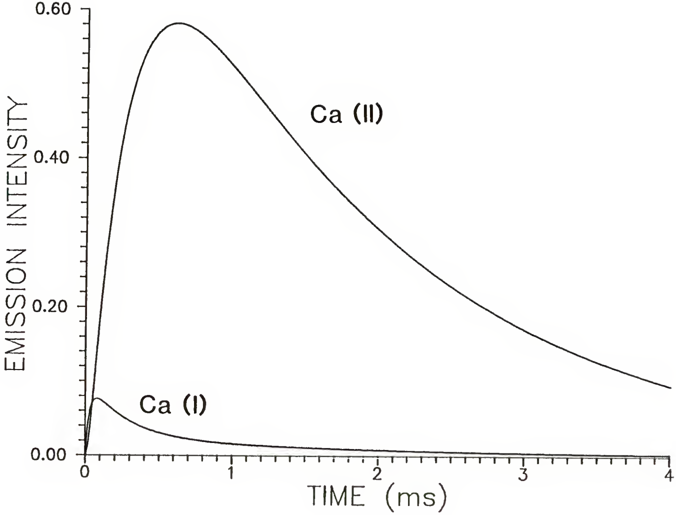
0.60
0.40
0.20
0.00
EMISSION INTENSITY
Ca (II)
Ca (I)
0
1
2
3
4
TIME (ms)

Fig. 24. Simulation of Ca atom distribution at various rf power.

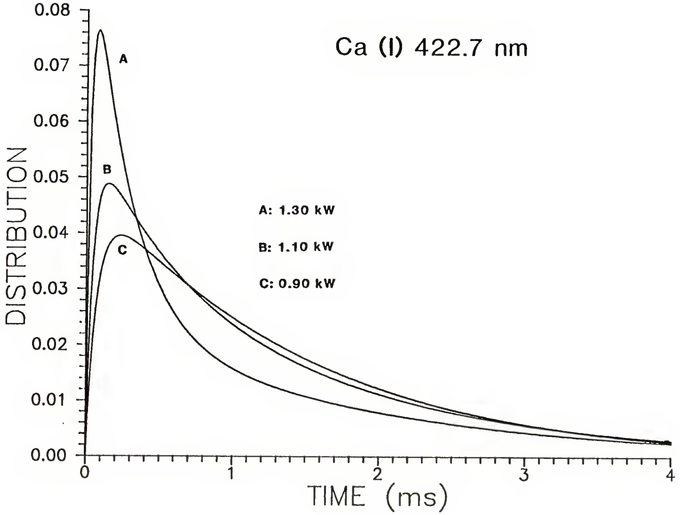
Ca (I) 422.7 nm
A: 1.30 kW
B: 1.10 kW
C: 0.90 kW
A
B
C
DISTRIBUTION
0.08
0.07
0.06
0.05
0.04
0.03
0.02
0.01
0.00
TIME (ms)
0
1
2
3
4

Fig. 25. Simulation of Ca ion distribution at various rf power.

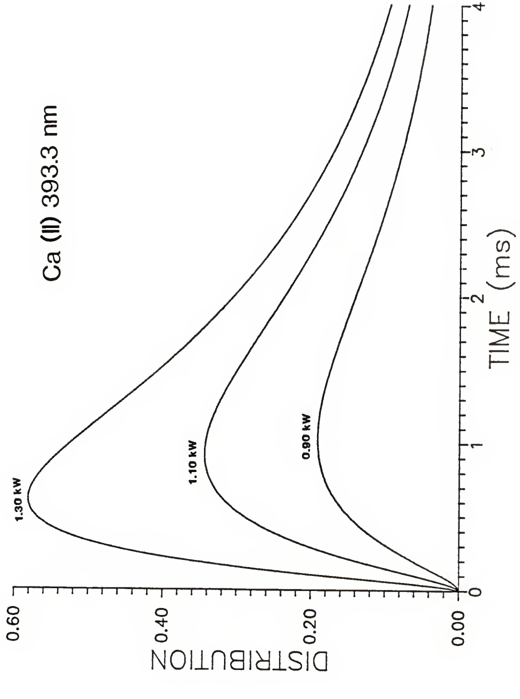
Ca (II) 393.3 nm
1.30 kW
1.10 kW
0.90 kW
DISTRIBUTION
0.60
0.40
0.20
0.00
0
1
2
3
4
TIME (ms)

$$K = \frac{k_I}{k_R} = \frac{n_i n_e}{n_a} = (2\pi mkT/h^2)^{3/2} \frac{2Z_i}{Z_a} \exp(-E_I/kT) \qquad (3\text{-}32)$$

where m, h, and k have their usual significance; Z is the electronic partition function; E_I is the ionization energy of the analyte; and T is the temperature. If Boltzmann equilibration among atomic and ionic levels is faster than Saha equilibration, the above equation implies that the ion-atom line ratio at a certain point in the plasma should be independent of analyte concentration. Table 2 gives the concentration dependence of Ca(II)/Ca(I) ratios at different heights. The variation in the Ca(II)/Ca(I) is far greater than experimental errors, demonstrating that Saha equilibrium is not reached at these positions. As indicated by Alkemade et al. [119], the Saha equation holds only for an unbounded plasma or a plasma surrounded by an inert wall of the same temperature, e.g., a shielded flame.

However, Mg shows a greater recombination rate, almost three times greater than Ca. The fast recombination results in narrowing the atom-ion peak separation, lowering the ion/atom ratio, and making the atom peak position invariant with power. Moreover, the Mg ion/atom ratio is also relatively independent of solution concentration (Table 3). The conditions of equilibrium include that the atom and ion profiles should have the same shape and position, that they should vary in the same manner with power, and that the Saha equation should hold (including an invariant Saha constant with

Table 2. Experimental Dependence of Ca(II)/Ca(I) Ratio[a,b] on Concentration of Calcium Aspirated.

Vertical Position (mm above coil)	Ca(II)/Ca(I) Ratio			
	Ca Concentration Aspirated			
	0.02 ppm	0.1 ppm	1 ppm	10 ppm
4	0.15	0.73	4.67	22.31
5	0.58	2.91	18.46	39.77
6	1.38	4.59	45.57	67.87
7	2.25	11.25	55.41	83.85
8	4.05	14.56	64.88	98.98
9	7.67	26.55	64.69	69.81
10	8.41	37.54	73.33	76.98
12	9.48	47.28	86.10	106.68
15	12.70	45.99	95.51	89.39

[a] Data obtained with a Plasma-Spec I (Leeman Labs, Lowell, MA); Ca(I) (422.67 nm) measured for 3s, Ca(II) (393.4 nm) measured for 1s.

[b] K.P. Li, private communication.

Table 3. Experimental Dependence of Mg(II)/Mg(I) Ratio[a,b] of Concentration of Magnesium Aspirated.

Vertical Position (mm above coil)	Mg(II)/Mg(I) Ratio			
	Mg Concentration Aspirated			
	0.02 ppm	0.1 ppm	1 ppm	10 ppm
4	29.85	5.94	4.31	4.39
5	23.47	7.51	6.16	6.08
6	11.63	6.66	6.02	5.90
7	8.62	6.44	6.08	6.19
8	7.58	6.25	5.99	5.83
9	8.83	7.25	6.89	6.84
10	8.43	7.25	6.89	6.84
11	8.83	7.39	7.04	6.76
12	9.06	7.10	6.76	6.59
13	8.61	7.24	6.90	6.72
15	9.13	6.96	6.49	6.40

[a] Data obtained with a Plasma-Spec I (Leeman Labs, Lowell, MA). Both Mg(I) (285.2 nm) and Mg(II) (279.5 nm) were integrated 3s.

[b] K.P. Li, private communication.

solution concentration). Magnesium is seen to be closer to chemical equilibrium in all aspects than calcium.

Both atom and ion spatial height distribution functions consist of exponentials of rate constants as indicated in Chapter 2. Processes with much greater rate constants will not be rate determining. The ionization rate constant, k_I, of calcium increases rapidly as the rf power increases. This implies that the influence of the ionization step in atom and ion distribution becomes less significant with the increase of rf power. Under normal operational conditions, the most influential step is most likely the dissociation of calcium oxide. Any means to speed up dissociation would enhance both atom and ion signals. An increase in recombination, on the other hand, would be more beneficial for atomic measurements. A shift in the atom profile would be expected in such changes. The magnesium situation is more difficult to predict because the influence of k_I cannot be neglected. Both chemical and physical interferences will be discussed in more details in the future work.

From simulated profiles of Ca, the atom distribution seems to peak too early compared to experimental ones. This may be attributed to the following factors. First, the simulation is based on droplets of a uniform size, whereas in the real system there is a finite range of droplet sizes. Each droplet size yields a slightly different distribution. By using the integral of these individual distributions, the overall signal profile may be distorted. Second, it is assumed that the vaporization takes an appreciable length of time to complete. This is demonstrated by the slowly rising leading edge in the molecular emission of yttrium (Fig. 26). The noninstantaneous release of oxide vapor delays the appearance of the profile maximum and broadens the distribution.

In conclusion, the estimation of k_X, k_D, and k_R may not be as precise or accurate as we prefer, but they do provide useful kinetic information about analyte processes in the plasma. Moreover, chemical and physical interferences can now be studied in a more quantitative manner.

Fig. 26. Molecular emission profile of yttrium (YO band: 597.2 nm).

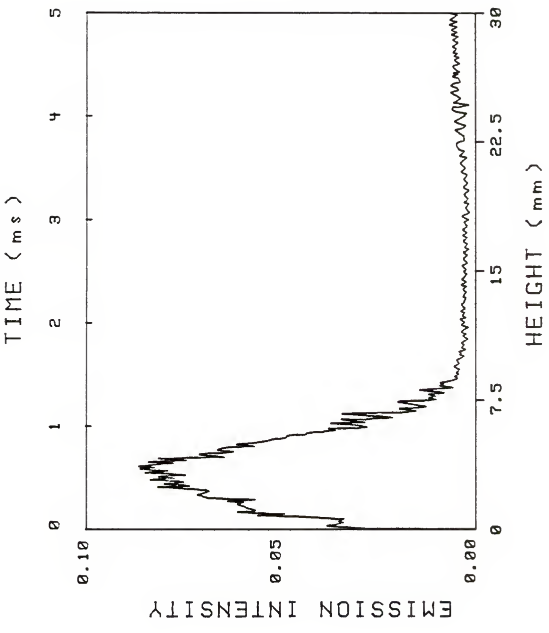
TIME (ms)
0
1
2
3
4
5
EMISSION INTENSITY
0.10
0.05
0.00
HEIGHT (mm)
0
7.5
15
22.5
30

CHAPTER 4
CONCLUSIONS AND FUTURE WORK

The dynamic model based on a stochastic approach through a single droplet distribution has been established. In this model, the axial distribution functions for the molecular, atomic, and ionic analyte species are explicitly characterized by their statistical moments. The zeroth and first moments are used for estimating rate constants of atomization (k_D), ionization (k_I), recombination (k_R), and vapor plume expansion (k_X). Only k_I can be estimated directly from the signal profiles. The expansion constant (k_X) can only vary within a narrow range. By using an educated guess for the value of k_X, rate constants k_I and k_R can be calculated. Two elements, calcium and magnesium, are used in this study. The power dependence of k_I for Ca is different from that for Mg. The fast increase in k_I vs rf power makes ionization less favorable as a rate-determining step in Ca excitation in high power. Magnesium has a k_I nearly independent of rf power. Its atomic and ionic profiles vary with power in the same manner, whereas Ca(I) profiles show a shift with power.

The computer simulated profiles (Figs. 27 and 28) are different from the experimental data attributing to several factors. The simulation is built on the assumption of uniform sized droplets,

Fig. 27. The comparison between the computer simulated distribution and the experimental spatial profiles of calcium atom at various rf power (from Figures 17 and 24).

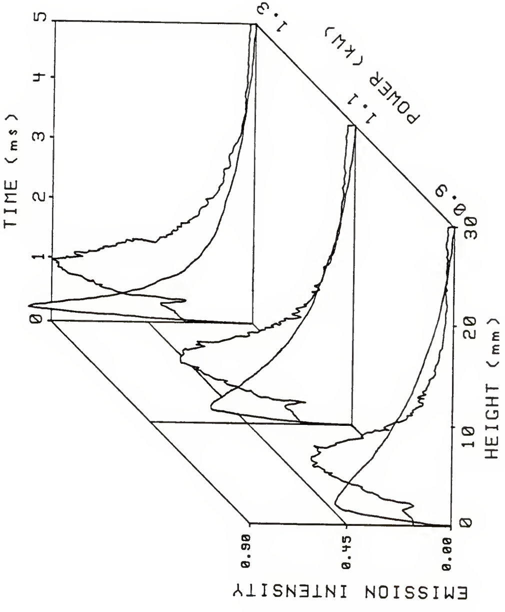
TIME (ms)
0
1
2
3
4
5
POWER (KW)
1.3
1.1
0.9
HEIGHT (mm)
0
10
20
30
EMISSION INTENSITY
0.00
0.45
0.90

Fig. 28. The comparison between the computer simulated distribution and the experimental spatial profiles of calcium ion at various rf power (from Figures 18 and 25).

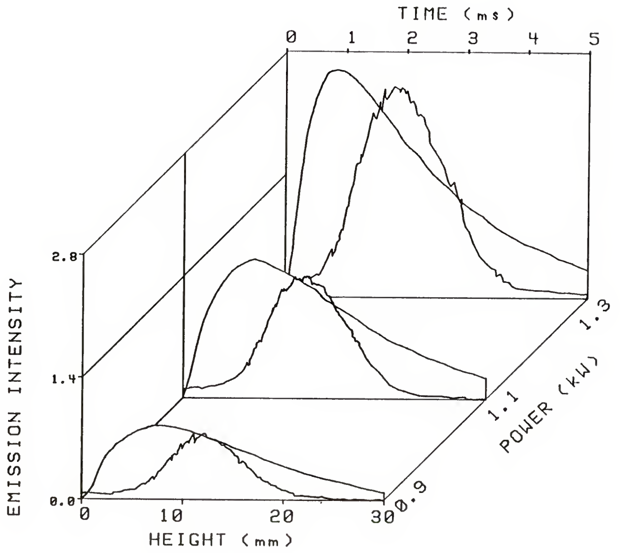
TIME (ms)
0
1
2
3
4
5
EMISSION INTENSITY
2.8
1.4
0.0
0
10
20
30
HEIGHT (mm)
0.9
1.1
1.3
POWER (kW)

whereas the real system has a finite range of droplet sizes. Different size droplets have distinct spatial distributions. This leads to the distortion of the overall signal profile. Another factor is that the vaporization also requires time to complete. The noninstantaneous release of molecular oxide emission delays the profile maximum and broadens the distribution.

In order to get better agreement between the experimental data and the computer simulation profiles, several modifications of the proposed model should be taken into consideration. First, a vaporization term should be added to the theoretical equation to adjust the starting point of the simulated distribution. Second, the droplet size distribution of the analyte species should be considered and/or better control of the droplet size using an improved droplet producing system (nebulizer, spray chamber and desolvation system). The consideration of the detailed droplet distributions relies upon a consideration of fluid dynamics and diffusion problems treated by Fick's law. Last, air entrainment is important at higher positions above the ICP torch. This is the reason why the experimental profile drops rapidly at heights of 20 mm above the loading coil. Therefore, the air entrainment factor should be put into the computer simulation equation to represent accurately the tailing of the measured profile. The inherent value of this research for understanding of the operation of the ICP depends upon the fitness of these modifications to the model in order to describe more accurately the real situation. Even so, the dissertation work represents the first attempt to model the production of atoms and ions as a function of height in the ICP.

Since k_I can directly be obtained from the experimental signal profiles, the other rate constants, so obtained through a series of estimated k_X values, can certainly be considered as reliable estimates. In addition to the rf power, the variation in experimental conditions, such as addition of interfering species (ethanol, Al, PO_4^{3-}, Na, EDTA, etc.), argon gas flow rate, solution uptake rate, etc., can also provide useful kinetic information through investigation of the changes in the four rate constants.

As mentioned in Chapter 2, a curve fit to the experimental spatial profiles can provide a set of coefficients. From these coefficients, the four rate constants can be estimated. This is also a direction for future studies.

The previous ICP mechanistic studies all focused on the excitation process and also all treated the ICP in a static mode with the LTE assumption. However, the basis of these models contradict the genuine conditions, namely, the ICP is not in LTE and also a dynamic system.

The model studied here is the first one which is concerned with the atomization and ionization mechanisms through a stochastic approach. In this model, all processes are considered in kinetic (dynamic) styles which lead to time- (height-) dependent distributions of analyte species. The spatially resolved distributions are characterized by their statistical moments. The evaluation of these moments allows us to estimate a number of reaction rate constants. By comparison of the modified simulated profiles using a set of rate constants with the measured distributions, analyte atomization and ionization can be more precisely and quantitatively predicated.

APPENDIX A
EXPANSION DUE TO ANALYTE DIFFUSION AND CHEMICAL REACTIONS

Under constant pressure and uniform temperature, volume expansion can be attributed to diffusion and/or chemical reactions generating more product particles than the reactant. They are discussed separately for a general reaction:

$$A \xrightarrow{k} \text{Products}$$

Expansion Due to Analyte Diffusion

Assuming that the vapor plume under investigation has a volume, V_0, at $t = 0$, then

$$V_0 = (4/3)\pi r_0^3 \tag{A-1}$$

where r_0 is the initial radius of the plume. After a certain time of diffusion, t, the radius of the plume is

$$r = r_0 + \sqrt{2Dt} = r_0(1 + m\sqrt{t}) \tag{A-2}$$

where D is the average diffusion coefficient (assume all analyte species have approximately the same diffusion coefficient) and

$m = \sqrt{2D}/r_0$ is a time-independent variable. The volume of the plume is thus

$$V = V_0(1 + m\sqrt{t})^3 \tag{A-3}$$

or

$$\ell n\ V = \ell n\ V_0 + 3\ \ell n\ (1 + m\sqrt{t}). \tag{A-4}$$

Differentiation gives

$$\frac{d\ \ell n\ V}{dt} = \frac{3m}{2(1 + m\sqrt{t})t^{1/2}} \tag{A-5}$$

Substitution into the rate equation [120]

$$\frac{d[A]}{dt} = -k[A] - [A]\frac{d\ \ell n\ V}{dt} \tag{A-6}$$

and integration with respect to t yields

$$[A] = [A]_0 \exp(-kt)/(1 + m\sqrt{t})^3 \tag{A-7}$$

where $[A]_0$ is the initial concentration of A.

Without expansion, the concentration would be

$$[A] = [A]_0\ \exp(-kt) \tag{A-8}$$

The correction factor is seen to be $(1 + m\sqrt{t})^{-3}$.

Volume Expansion Due to Chemical Reactions

For simplicity, only dissociation of a diatomic species will be considered here. Using y to denote the fraction of dissociation, i.e.,

$$y = \frac{[A]_0 - [A]}{[A]_0 + [A]} \quad \text{(A-9)}$$

the volume of the reaction mixture will be

$$V = V_0(1 + y)$$

and

$$\frac{d \ln V}{dt} = \frac{1}{1 + y} \frac{dy}{dt} \quad \text{(A-10)}$$

Substituting this into the rate equation and integrating with respect to t, one obtains

$$[A] = [A]_0 \exp(-kt)/(2 - \exp(-kt)) \quad \text{(A-11)}$$

The correction factor is therefore $[2 - \exp(-kt)]^{-1}$.

If the vapor plume expands due to both diffusion and dissociation, the overall correction will be the product of the above factors, i.e., $(1 + m\sqrt{t})^{-3}[2 - \exp(-kt)]^{-1}$. This is a relatively complicated factor. It will become more involved if other processes are taken into consideration and, eventually, it will become impossible to solve the rate equations explicitly. However, when this function is replaced by an approximation function, such as $\exp(-k_X t)$, with k_X as the expansion rate constant, the situation is greatly simplified. The rate equation is now

$$\frac{d[A]}{dt} = -(k + k_X)[A] \qquad \text{(A-12)}$$

It is generally possible to fit a set of monotonically increasing or decreasing data with an exponential function. The above manipulation is quite acceptable. Figure 29 shows the discrepancy between $\exp(-k_X t)$ and the correction factor. Evidently the fitting is reasonably good except at lower height.

Fig. 29. Discrepancy between $\exp(-k_X t)$ and the function $(1 - m\sqrt{t})^{-3}[2 - \exp(-kt)]^{-1}$ simulated with a set of hypothetical constants: $k_X = 10\ \mathrm{ms}^{-1}$, $m = 5\ \mathrm{ms}^{-1/2}$, and $k = 1\ \mathrm{ms}^{-1}$.

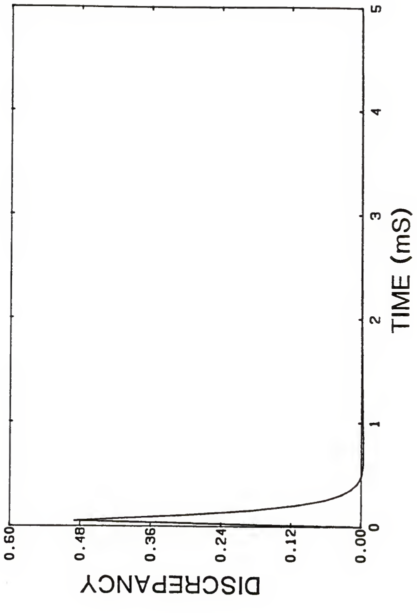
DISCREPANCY
0.60
0.48
0.36
0.24
0.12
0.00
0
1
2
3
4
5
TIME (mS)

APPENDIX B
SOLUTION OF RATE CONSTANTS

The rates of radiative transitions between atomic and ionic levels are normally much faster than the rates of molecular dissociation, ionization, and recombination. Therefore, it is conceivable that these excitation processes can be assumed to be at steady state, i.e.,

$$M^{*} / M = k^{*}_{E,A} / k^{*}_{R,A} = k^{*}$$

and

$$M^{+*} / M^{+} = k^{*}_{E,I} / k^{*}_{R,I} = k^{+*}$$

Denoting the number densities of MX, M, and M^{+} as n_m, n_a, and n_i, respectively, the rate equations for the simplified scheme (Fig. 2(B)) can be expressed as follows:

$$dn_m/dt = -k_D n_m - k_X n_m \qquad (B-1)$$

$$dn_a/dt = k_D n_m - k_I n_a + k_R n_i - k_X n_a \qquad (B-2)$$

$$dn_i/dt = k_I n_a - k_R n_i - k_X n_i \qquad (B-3)$$

Providing the expansion has the same effect to all species in the plasma, k_X is an apparent function of diffusion coefficients.

The boundary conditions can be set

$$n_m = n_0,\ n_a = n_i = 0 \qquad \text{at } t = 0$$

$$n_m = n_a = n_i = 0 \qquad \text{at } t = \infty$$

Taking Laplace transformation, the above three equations give

$$s\bar{n}_m - n_0 = -(k_D+k_X)\bar{n}_m \tag{B-4}$$

$$s\bar{n}_a = k_D\bar{n}_m - (k_I+k_X)\bar{n}_a + k_R\bar{n}_i \tag{B-5}$$

$$s\bar{n}_i = k_I\bar{n}_a - (k_R+k_X)\bar{n}_i \tag{B-6}$$

where s is the dummy parameter for Laplace transformation. From Eq. (B-4), we get

$$\bar{n}_m = n_0/(s+k_D+k_X) \tag{B-7}$$

Taking the inversion of Laplace transformation of Eq. (B-7), we get

$$n_m = n_0\exp[-(k_D+k_X)t] \tag{B-8}$$

Rearranging Eq. (B-6) yields

$$(s+k_R+k_X)\bar{n}_i = k_I\bar{n}_a \tag{B-9}$$

or

$$\bar{n}_i = k_I\bar{n}_a/(s+k_R+k_X) \tag{B-10}$$

Substituting Eq. (B-10) into Eq. (B-5) gives

$$(s+k_I+k_X)\bar{n}_a = k_D\bar{n}_m + k_Ik_R\bar{n}_a/(s+k_R+k_X)$$

or

$$[s+k_I+k_X-k_Ik_R/(s+k_R+k_X)]\bar{n}_a = k_D\bar{n}_m = k_Dn_0/(s+k_D+k_X)$$

The common denominator of the left side yields

$$[s^2+(k_I+k_R+2k_X)s + k_X(k_I+k_R+k_X)]\bar{n}_a/(s+k_R+k_X) = k_Dn_0/(s+k_D+k_X) \tag{B-11}$$

Let $a = k_D+k_X$, $d = k_R+k_X$, $\alpha = k_I+k_R+2k_x$, and $\beta = k_X(k_I+k_R+k_X)$. Then Eq. (B-11) becomes

$$(s^2+\alpha s+\beta)\bar{n}_a/(s+d) = k_Dn_0/(s+a)$$

Rearranging the above equation yields

$$\bar{n}_a = k_D(s+d)n_0/[(s+a)(s^2+\alpha s+\beta)] \tag{B-12}$$

The denominator of the right side of the Eq. (B-12) can separate three items,

$$\bar{n}_a = k_D(s+d)n_0/[(s+a)(s+b)(s+c)] \qquad \text{(B-13)}$$

where

$$b = [\alpha-(\alpha^2-4\beta)^{1/2}]/2$$

and

$$c = [\alpha+(\alpha^2-4\beta)^{1/2}]/2$$

Substituting Eq. (B-13) into Eq. (B-10) yields

$$\bar{n}_i = k_I\bar{n}_a/(s+d) = k_Ik_Dn_0/[(s+a)(s+b)(s+c)] \qquad \text{(B-14)}$$

In Eqs. (B-13) and (B-14), the s (Laplacian parameter) related items can be separated; several items depend on the items of denominator. These are

$$(s+d)/[(s+a)(s+b)(s+c)] = A/(s+a) + B/(s+b) + C/(s+c) \qquad \text{(B-15)}$$

and

$$[(s+a)(s+b)(s+c)]^{-1} = D/(s+a) + E/(s+b) + F/(s+c) \qquad \text{(B-16)}$$

where

$$A = (d-a)/[(a-b)(a-c)] \tag{B-17}$$

$$B = (b-d)/[(a-b)(b-c)] \tag{B-18}$$

$$C = (d-c)/[(a-c)(b-c)] \tag{B-19}$$

$$D = [(a-b)(a-c)]^{-1} \tag{B-20}$$

$$E = [(a-b)(b-c)]^{-1} \tag{B-21}$$

and

$$F = [(a-c)(b-c)]^{-1} \tag{B-22}$$

Substituting Eq. (B-15) into Eq. (B-13) and take the inversion of Laplace transformation, we get

$$n_a = k_D n_0[A\exp(-at)+B\exp(-bt)+C\exp(-ct)] \tag{B-23}$$

Substituting Eq. (B-16) into Eq. (B-14) and taking the inversion of Laplace transformation, we get

$$n_i = k_I k_D n_0[D\exp(-at)+E\exp(-bt)+F\exp(-ct)] \tag{B-24}$$

APPENDIX C
PROGRAM FOR COMPUTER SIMULATION

```
10   REM ICP SIMULATION
20   REM KD-DECOMPOSITION, KI-IONIZATION
30   REM KR-RECOMBINATION, KE-EXPANSION
40   INPUT "INPUT KD";KD
50   INPUT "INPUT KI";KI
60   INPUT "INPUT KR";KR
70   INPUT "INPUT KE";KE
80   INPUT "INPUT FILE NAME, LESS THAN 7 CHARACTERS"; FILE$
90   NAME1$=FILE$+"A.DAT"
100  NAME2$=FILE$+"I.DAT"
110  OPEN NAME1$ FOR OUTPUT AS#1
120  OPEN NAME2$ FOR OUTPUT AS#2
130  REM CALCULATIONS
140  AA=KD+KE
150  BB=KI+KR+2*KE
160  CC=KE*(KI+KR+KE)
170  DD=KR+KE
180  M=(BB-SQR(BB*BB-4*CC))*.5
190  N=(BB+SQR(BB*BB-4*CC))*.5
200  X=AA-M
210  Y=AA-N
220  Z=M-N
230  D=1/(X*Y)
240  A=(DD-AA)*D
250  E=-1/(X*Z)
260  B=-(M-DD)*E
270  F=1/(Y*Z)
280  C=(DD-N)*F
290  INPUT "X-AXIS IN MS. (DFLT=5)";CONSTANT$:CONSTANT=VAL(CONSTANT$)
300  IF LEN(CONSTANT$)=0 THEN CONSTANT=5
310  PRINT "BE PATIENT! IT'S CALCULATING!"
320  FOR I=0 TO 249
330  T=CONSTANT/249*I
340  N2=KD*(A*EXP(-AA*T)+B*EXP(-M*T)+C*EXP(-N*T))
350  N3=KI*KD*(D*EXP(-AA*T)+E*EXP(-M*T)+F*EXP(-N*T))
360  PRINT #1,N2
370  PRINT #2,N3
380  NEXT I
390  CLS
400  PRINT "IT'S DONE"; INPUT "WANT ANOTHER RUN ? YES OR NO"; Y$
410  IF Y$="Y" THEN 40
420  PRINT "END"
430  END
```

APPENDIX D
PROGRAM FOR STATISTICAL MOMENTS CALCULATION

```
C              PROGRAM MOMENT
C***********************************************************
C***           INPUT A RAMP DATA INTO SR265(BINARY)      ***
C***           FOR MOMENT CALCULATIONS                   ***
C***********************************************************
      INTEGER*4 NBINS,FACTOR
         REAL*4 XRLMIN,XRLMAX,YRLMIN,YRLMAX,SFCTR,SINIT
         LOGICAL*4 RAWDAT,RATIO,SCL
         CHARACTER*4 SCLSTR
         INTEGER*2 OLDPT(2100)

         OPEN(10,FILE='MOMENT.DAT',STATUS='NEW',FORM='BINARY')
         RAWDAT=.FALSE.
         NBINS=2000
         RATIO=.TRUE.
         FACTOR=1
         XRLMIN=1
         XRLMAX=2000
         YRLMIN=-2048
         YRLMAX=2048
         SCL=.FALSE.
         SFCTR=1
         SINIT=1
         SCLSTR='BINS'
         WRITE(10)RAWDAT,NBINS,RATIO,FACTOR,XRLMIN,XRLMAX,YRLMIN,
    C    YRLMAX,SCL,SFCTR,SINIT,SCLSTR

         DO 20 I=1,2100
         OLDPT(I)=I
         WRITE(10)OLDPT(I)
20    CONTINUE
         CLOSE(10)
         STOP
         END
```

APPENDIX E
PROGRAM TO CALCULATE RATE CONSTANTS IN INDUCTIVELY COUPLED PLASMA

```
10    REM             PROGRAM RATE2
20    REM            *****************************************
30    REM            *                                       *
40    REM            *       Program to calculate            *
50    REM            *       rate constants of ICP           *
60    REM            *                                       *
70    REM            *****************************************
80    CLS
90    INPUT "File name of atom=";ATOM$
100   INPUT "File name of ion=";ION$
105   INPUT "Element, Conc., Power";ECP$
110   INPUT "Zeroth moment of atom=";A0
120   INPUT "First moment of atom=";A1
130   INPUT "Zeroth moment of ion=";I0
140   INPUT "First moment of ion=";I1
160   REM conversion of bins to time(ms)
170   INPUT "1:approximation, 1400 bins=5 ms; 2:by calculation";CONV
180   IF CONV=2 THEN GOTO 230
190        T=280
200   GOTO 330
210   PRINT
220   PRINT
230   INPUT "Distance scanned in cm";DIS
240   INPUT "Torch diameter in cm";DIA
250   INPUT "Gas flow rate in liter/min";FLO
260   INPUT "Bin number",BIN
270   REM lin=linear velocity; flow rate calibrated by volume
           expansion at 5000 C
280        FLO1=FLO*1/60
290   REM apply gas law
300        LIN=(FLO1*5000/300)/<.25*DIA*DIA*3.14)
310   TIME=DIS/LIN
320   T=BIN/TIME
330          SA=A1/A0
340          SI=I1/I0
350          SI1=I1/I0
380          D=1/(SI-SA)
390          KI=D*I0/A0
400          B=KI+D
```

```
410          B1=1/B
420          W=SI-B1
425          KI1=KI
430   LPRINT
434   LPRINT
440   LPRINT CHR$(14);"File name of atom: ";ATOM$
445   LPRINT CHR$(14);"File name of ion: ";ION$
449   LPRINT
454   LPRINT CHR$(18);"Element, Conc. Power"
459   LPRINT CHR$(14); ECP$
465   LPRINT
469   LPRINT CHR$(18);"Zeroth moment of atom profile=";A0
475   LPRINT "First moment of atom profile=";A1
479   LPRINT "Center of gravity of atom profile=";SA
480   LPRINT "Zeroth Moment of ion profile=";I0
485   LPRINT "Center of gravity of ion profile=";SI
490   LPRINT "First moment of ion profile=";I1
520          F=1.05
530          FOR I=1 TO 20
540          AL=F/W
550          AC=AL*(2-W*AL)/(W*AL-1)
560          KI=KI1*T
570          KX=AL*T
580          KD=AC*T
590          KR=(D-AL)*T
614   LPRINT
615   LPRINT
617   LPRINT "Dissociation Factor=";F
620   LPRINT "Dissociation constant (mS), Kd=";KD
630   LPRINT "Ionization constant (mS), Ki=";KI
640   LPRINT "Recombination constant, Kr=";KR
650   LPRINT "Expansion rate constant (mS), Kex=";KX
660   LPRINT
670   LPRINT
680   LPRINT
690   PRINT
700          F=F+.05
710          NEXT I
720   INPUT "Need another run?";Y1$
730          IF Y1$="y" THEN GOTO 80
740          PRINT "END"
750             END
```

APPENDIX F
PROGRAM FOR GETTING DATA FROM SR 265 BINARY TO ASCII

```
C                        program getdat
C                ************************************************
C                **                                             **
C                **           Get data from SR 265              **
C                **           Binary to ASCII                   **
C                **                                             **
C                ************************************************
                 INTEGER*4 NBINS,FA
                 INTEGER*2 PT(2000)
                 LOGICAL*4 RA,RB,SA
                 REAL*4 XA,XB,YA,YB,SB,SC,T
                 CHARACTER*4 SD
                 CHARACTER*1 ANS
   5          OPEN(10,FILE=' ',STATUS='OLD',FORM='BINARY')
                 READ(10)RA,NBINS,RB,FA,XA,XB,YA,YB,SA,SB,SC,SD,
     1   (PT(I),I=1,NBINS)
                 CLOSE(10)
                 OPEN (12,FILE=' ',STATUS='NEW ',ACCESS='SEQUENTIAL')
C                TIME INTERVAL FOR X AXIS
                 T=5.0/REAL(NBINS)
                 DO 20 J=1,NBINS,5
                 X=J*T
                 Y=REAL(PT(J))/400
                 WRITE(12,30) X,Y
   30            FORMAT(F6.3,5X,E10.3)
   20         CONTINUE
                 CLOSE(12)
                 WRITE(*,*) '     WANT ANOTHER RUN?'
                 READ (*,60) ANS
   60            FORMAT(1A)
                 IF(ANS.EQ.'Y') GOTO 5
                 STOP
                 END
```

REFERENCES

1. G.I. Babat, Vestn. Elektroprom., No. 2, 1; No. 3, 2 (1942).
2. G.I. Babat, J. Inst. Elec. Engrs. (London), 94, 27 (1947).
3. T.B. Reed, J. Appl. Phys., 32, 821 (1961).
4. T.B. Reed, J. Appl. Phys., 32, 2534 (1961).
5. T.B. Reed, Int. Sci. Technol., 6, 42 (1962).
6. V.A. Fassel, ICP Information Newslett., 1, 267 (1976).
7. V.A. Fassel, Anal. Chem., 51, 1290A (1979).
8. S. Greenfield, ICP Information Newslett., 1, 3 (1975).
9. S. Greenfield, I.L.W. Jones and C.T. Berry, Analyst, 89, 713 (1964).
10. R.H. Wendt and V.A. Fassel, Anal. Chem., 37, 920 (1965).
11. S. Greenfield, C.T. Berry and L.G. Bunch, Spectroscopy with a High Frequency Plasma Torch, Radyne International, Wokingham, England (1965).
12. S. Greenfield, I.L.W. Jones and C.T. Berry, U.S. Patent 3,467,471, September 16, 1969.
13. S. Greenfield, I.L.W. Jones, C.T. Berry and L.G. Bunch, Proc. Soc. Anal. Chem., 2, 111 (1965).
14. G.W. Dickinson and V.A. Fassel, Anal. Chem., 41, 1021 (1969).
15. V.A. Fassel, Proc. 16th Coll. Spectr. Int., Heidelberg 1971, Plenary lectures and reports, Adam Hilger, London (1972), p. 63.
16. R.H. Wendt and V.A. Fassel, Anal. Chem., 38, 337 (1966).
17. H.C. Hoare and R.A. Mostyn, Anal. Chem., 39, 1153 (1967).
18. M.E. Britske, V.M. Borisov and Yu.S. Sukah, Ind. Lab., 33, 301 (1967).

19. J.M. Mermet and J. Robin, Proc. 14th Coll. Spectr. Int., Debrecen 1967, Vol. 2, Hilger, London (1968), p. 715.

20. R.M. Barnes, Emission Spectroscopy, Dowden, Hutchinson & Ross, Stroudsburg, PA (1976).

21. H. Dunken and G. Pforr, Z. Phys. Chem., 230, 48 (1965).

22. G. Pforr, Proc. 14th Coll. Spectr. Int., Debrecen 1967, Vol. 2, Hilger, London (1968), p. 687.

23. C. Bordonali and M.A. Biancifiori, Met. It., No. 8, 631 (1967).

24. C. Bordonali and M.A. Biancifiori, Proc. 14th Coll. Spectr. Int., Debrecen 1967, Vol. 3, Hilger, London (1968), p. 1153.

25. V.M. Gold'farb and V.K. Goikhman, J. Appl. Spectrosc. USSR, 8, 119 (1968).

26. I. Kleinmann and V. Svoboda, Anal. Chem., 41, 1029 (1969).

27. G.H. Morrison and Y. Talmi, Anal. Chem., 42, 809 (1970).

28. D. Truitt and J.W. Robinson, Anal. Chim. Acta, 49, 401 (1970); 51, 61 (1970).

29. J.C. Souilliart and J. Robin, Analusis, 1, 427 (1972).

30. P.W.J.M. Boumans and F.J. de Boer, Spectrochim. Acta, 27B, 391 (1972).

31. V.A. Fassel and R.N. Kniseley, Anal. Chem., 46, 1110A, 1155A (1974).

32. P.W.J.M. Boumans and F.J. de Boer, Spectrochim. Acta, 30B, 309 (1975).

33. R.H. Scott, V.A. Fassel, R.N. Kniseley and R.N. Nixon, Anal. Chem., 46, 75 (1974).

34. J.M. Mermet, C.R. Acad. Sci. Ser. B, 281, 273 (1975).

35. S. Greenfield, H.McD. McGeachin and P.B. Smith, Talanta, 23, 1 (1976).

36. S. Greenfield, I.L.W. Jones, H.McD. McGeachin and P.B. Smith, Anal. Chim. Acta, 74, 225 (1975).

37. A. Montaser, V.A. Fassel and J. Zalewski, Appl. Spectrosc., 35, 292 (1981).

38. A. Montaser and J. Mortazavi, Anal. Chem., 52, 255 (1980).

39. L. Ebdon, M.R. Cave and D.J. Mowthorpe, Anal. Chim. Acta, 115, 179 (1980).

40. G.L. Moore, P.J. Humphries-Cuff and A.E. Watson, Spectrochim. Acta, 39B, 915 (1984).

41. A.E. Watson and G.M. Russell, Report No. 1907. National Institute of Metallurgy, Randburg, South Africa (1977); ICP Information Newslett., 3, 273 (1977).

42. A.E. Watson and G.M. Russell, Report No. 1934. National Institute of Metallurgy, Randburg, South Africa (1977); ICP Information Newslett., 3, 409 (1978).

43. A.E. Watson and T.W. Steele, Report No. 2029. National Institute of Metallurgy, Randburg, South Africa (1977); ICP Information Newslett., 5, 553 (1980).

44. K. Ohls and D. Sommer, ICP Information Newslett., 4, 532 (1979).

45. D. Sommer and K. Ohls, Fresenius Z. Anal. Chem., 295, 337 (1979).

46. K. Ohls and D. Sommer, Fresenius Z. Anal. Chem., 296, 241 (1979).

47. A. Aziz, J.A.C. Broekaert and F. Leis, Spectrochim. Acta, 37B, 369 (1982).

48. J.A.C. Broekaert, F. Leis and K. Laqua, Fresenius Z. Anal. Chem., 301, 105 (1980).

49. A. Aziz, J.A.C. Broekaert and F. Leis, Spectrochim. Acta, 36B, 251 (1981).

50. J.A.C. Broekaert, F. Leis and K. Laqua, in R.M. Barnes, ed., Developments in Atomic Plasma Spectrochemical Analysis, Heyden, London/Philadelphia (1981), p. 84.

51. J.A.C. Broekaert, F. Leis and G. Dincler, Analyst, 108, 717 (1983).

52. C.C. Butler, R.N. Kniseley and V.A. Fassel, Anal. Chem., 47, 825 (1975).

53. P.W.J.M. Boumans and F.J. de Boer, Proc. Anal. Div. Chem. Soc., 12, 140 (1975).

54. R.N. Kniseley, V.A. Fassel and C.C. Butler, Clin. Chem., 19, 801 (1973).

55. D.E. Nixon, V.A. Fassel and R.N. Kniseley, Anal. Chem., 46, 210 (1974).

56. A.L. Davison, J.R. Bethune and R.M. Ajhar, 24th Pittsburgh Conf. Anal. Chem. and Appl. Spectrosc., Abstr. Paper No. 30 (1973).

57. J.L. Jones, R.L. Dahlquist, J.W. Knoll and R.H. Hoyt, 24th Pittsburgh Conf. Anal. Chem. and Appl. Spectrosc., Abstr. Paper No. 147 (1974).

58. J.D. Winefordner, J.J. Fitzgerald and N. Omenetto, Appl. Spectrosc., 29, 369 (1975).

59. P.W.J.M. Boumans, Z. Anal. Chem., 279, 1 (1976).

60. B.L. Sharp, Sel. Anal. Rev. Anal. Sci., 4, 37 (1976).

61. V.A. Fassel, Pure Appl. Chem., 49, 1533 (1977).

62. R.M. Barnes, Trends Anal. Chem. (TrAC), 1, 51 (1981).

63. J.M. Mermet, Spectrochim. Acta, 30B, 383 (1975).

64. M.W. Blades and G. Horlick, Spectrochim. Acta, 36B, 861 (1981).

65. H. Kawaguchi, T. Ito and A. Mizuike, Spectrochim. Acta, 36B, 615 (1981).

66. P.W.J.M. Boumans and F.J. de Boer, Spectrochim. Acta, 32B, 365 (1977).

67. J.P. Rybarczyk, C.P. Jester, D.A. Yates, and S.R. Koirtyohann, Anal. Chem., 54, 2162 (1982).

68. P.E. Walters, T.L. Chester, and J.D. Winefordner, Appl. Spectrosc., 31, 1 (1977).

69. G.R. Kornblum and L. de Galan, Spectrochim. Acta, 32B, 71 (1977).

70. H.U. Eckert, Spectrochim. Acta, 33B, 591 (1978).

71. J.F. Alder, R.M. Bombelka, and G.F. Kirkbright, Spectrochim. Acta, 35B, 163 (1980).

72. W.H. Gunter, K. Visser, and P.B. Zeeman, Spectrochim. Acta, 37B, 571 (1982).

73. Y. Nojiri, K. Tanabe, H. Uchida, H. Haraguchi, K. Fuwa, and J.D. Winefordner, Spectrochim. Acta, 38B, 61 (1983).

74. J. Jorosz and J.M. Mermet, J. Quant. Spectrosc. Radia. Transfer, 17, 237 (1977).

75. T.E. Edmonds and G. Horlick, Appl. Spectrosc., 31, 536 (1977).

76. H. Uchida, K. Tanabe, Y. Nojiri, H. Haraguchi, and K. Fuwa, Spectrochim. Acta, 35B, 881 (1980).

77. H. Uchida, K. Tanabe, Y. Nojiri, H. Haraguchi, and K. Fuwa, Spectrochim. Acta, 36B, 711 (1981).

78. J.P. Robin, Prog. Anal. Atom. Spectrosc., 5, 79 (1982).

79. L. de Galan, Spectrochim. Acta, 39B, 537 (1984).

80. D.C. Schram, I.J.M.M. Raaymakers, B. van der Sijde, H.J.W. Schenkelaars, and P.W.J.M. Boumans, Spectrochim. Acta, 38B, 1545 (1983).

81. J.A.C. Broekaert, F. Leis, and K. Laqua, Spectrochim. Acta, 34B, 73 (1979).

82. P.W.J.M. Boumans, Spectrochim. Acta, 37B, 75 (1982).

83. T. Fujimoto, J. Phys. Soc. Jpn., 47, 265 (1979).

84. T. Fujimoto, J. Phys. Soc. Jpn., 47, 273 (1979).

85. T. Fujimoto, J. Phys. Soc. Jpn., 49, 1561 (1980).

86. T. Fujimoto, J. Phys. Soc. Jpn., 49, 1569 (1980).

87. F. Aeschbach, Spectrochim. Acta, 37B, 987 (1982).

88. M.W. Blades and G.M. Hieftje, Spectrochim. Acta, 37B, 191 (1982).

89. M.W. Blades, Spectrochim. Acta, 37B, 869 (1982).

90. J.W. Mills and G.M. Hieftje, Spectrochim. Acta, 39B, 859 (1984).

91. R.J. Lovett, Spectrochim. Acta, 37B, 969 (1982).

92. B. van der Sijde, H.M.J. Willems, and D.C. Schram, Proc. 16th ICPIG, Düsseldorf, BRD (1983).

93. T. Hasegawa, K. Fuwa, and H. Haraguchi, Chem. Lett., 2027 (1984).

94. G.M. Hieftje, G.D. Rayson, and J.W. Olesik, Spectrochim. Acta, 40B, 167 (1985).

95. T. Hasegawa and H. Haraguchi, Spectrochim. Acta, 40B, 1067, 1505 (1985).

96. T. Hasegawa, Ph.D. Dissertation, University of Tokyo (1985).

97. G.R. Kornblum and J. Smeyers-Verbeke, Spectrochim. Acta, 37B, 83 (1982).

98. I.J.M.M. Raaijmakers, P.W.J.M. Boumans, B. van der Sijde, and D.C. Schram, Spectrochim. Acta, 38B, 697 (1983).

99. B.L. Caughlin and M.W. Blades, Spectrochim. Acta, 39B, 1583 (1984).

100. F. Aeschbach, ICP Information Newslett., 6, 272 (1980).

101. N. Furuta and G. Horlick, Spectrochim. Acta, 37B, 53 (1982).

102. R.M. Barnes, CRC Crit. Rev. Anal. Chem., 7, 203 (1978).

103. E.H. Choot and G. Horlick, Spectrochim. Acta, 41B, 889, 935 (1986).

104. B.L. Caughlin and M.W. Blades, Spectrochim. Acta, 40B, 987 (1985).

105. W.H. Gunter, K. Visser, and P.B. Zeeman, Spectrochim. Acta, 38B, 949 (1983).

106. P.E. Walters, J.A. Lanauze, and J.P. Winefordner, Spectrochim. Acta, 39B, 125 (1984).

107. R.S. Houk and J.A. Olivares, Spectrochim. Acta, 39B, 575 (1984).

108. R.M. Barnes and R.G. Schleich, Spectrochim. Acta, 36B, 81 (1981).

109. S.W. Dowey, G.L. Keaton, and N.S. Nogar, Spectrochim. Acta, 40B, 927 (1985).

110. K.K. Chan, M.B. Bolger, and K.S. Pang, Anal. Chem., 57, 2145 (1985).

111. D.J. Kalnicky, V.A. Fassel, and R.N. Kniseley, Appl. Spectrosc., 31, 137 (1977).

112. J. Jarosz, J.M. Mermet, and J.P. Robin, Spectrochim. Acta, 33B, 55 (1978).

113. L.P. Hart, B.W. Smith, and N. Omenetto, Spectrochim. Acta, 41B, 1367 (1986).

114. N. Furuta, Spectrochim. Acta, 40B, 1013 (1985).

115. J.A. Kerr and A.F. Trotman-Dickenson, "CRC Handbook of Chemistry and Physics," 62, F180, CRC Press, Inc., Boca Raton, FL (1981).

116. K. Yamaoka and T. Nakagawa, J. Chromatogr., 92, 213 (1974).

117. D.J. Cutler, J. Pharm. Pharmacol., 30, 476 (1978).

118. D.A. McQuarrie, J. Chem. Phys., 38, 437 (1963).

119. C.Th.J. Alkemade, Tj. Hollander, W. Snelleman, and P.J.Th. Zeegers, "Metal Vapors in Flames," Pergamon, Oxford (1982).

120. G.B. Skinner, "Introduction to Chemical Kinetics," p. 20, Academic Press, New York (1974).

BIOGRAPHICAL SKETCH

Kigh-Shone Yeah was born on April 28, 1947, in Swatow, Kwantung, Republic of China (R.O.C.). He received his degree of Bachelor of Science in chemistry from Chung-Chen Institute of Technology (C.C.I.T.), Taoyuan, Taiwan, R.O.C., in August, 1970. After 2 years as a teaching assistant, he attended the graduate school in chemistry of C.C.I.T. In July, 1974, he received the degree of Master of Science in proton and phosphorus-31 Nuclear Magnetic Resonance (NMR) studies. Since that time, he has worked in the Chemical Analysis Center of Institute of Nuclear Energy Research. During the past 8 years (1974-1982), he has had working experiences in NMR (Varian T-60), Gas Chromatography-Mass Spectrometry (AEI-MS30), Arc and Spark Emission Spectrograph (Jarrell-Ash 3.4 m Ebert), and Dual Source Vacucomp$_{(TM)}$ (Jarrell-Ash 750 Electronically Controlled Waveform Source (ECWS) and Inductively Coupled Argon Plasma (ICAP) Dual Source Vacuum Emission Spectrometer). He began to work toward the Ph.D. degree at the University of Florida in August, 1982, under the supervision of Dr. James D. Winefordner.

He married Pearl Li-Ju Yu in 1977 and is the father of a 9-year-old son, Jun-Bo, and a 6-year-old daughter, Fung-I.

I certify that I have read this study and that in my opinion it conforms to acceptable standards of scholarly presentation and is fully adequate, in scope and quality, as a dissertation for the degree of Doctor of Philosophy.

James D Winefordner
James D. Winefordner, Chairman
Graduate Research Professor of Chemistry

I certify that I have read this study and that in my opinion it conforms to acceptable standards of scholarly presentation and is fully adequate, in scope and quality, as a dissertation for the degree of Doctor of Philosophy.

Joseph J Delfino
Joseph J. Delfino
Professor of Environmental Engineering Sciences

I certify that I have read this study and that in my opinion it conforms to acceptable standards of scholarly presentation and is fully adequate, in scope and quality, as a dissertation for the degree of Doctor of Philosophy.

Richard A Yost
Richard A. Yost
Associate Professor of Chemistry

This dissertation was submitted to the Graduate Faculty of the Department of Chemistry in the College of Liberal Arts and Sciences and to the Graduate School and was accepted as partial fulfillment of the requirements for the degree of Doctor of Philosophy.

August 1987

Dean, Graduate School